New insights into Late Pleistocene glacial and postglacial history of northernmost Ungava (Canada) from Pingualuit Crater Lake sediments

Hervé Guyard [a,b,*], Guillaume St-Onge [a,b], Reinhard Pienitz [c], Pierre Francus [b,d], Bernd Zolitschka [e], Garry K.C. Clarke [f], Sonja Hausmann [g], Veli-Pekka Salonen [h], Patrick Lajeunesse [c], Grégoire Ledoux [c], Michel Lamothe [i]

[a] Canada Research Chair in Marine Geology, Institut des sciences de la mer de Rimouski (ISMER), UQAR, Rimouski, Canada
[b] GEOTOP Research Center, Canada
[c] Centre d'études nordiques (CEN) & Département de Géographie, Université Laval, Québec, Canada
[d] Institut National de la Recherche Scientifique − Centre Eau, Terre, Environnement, Québec, Canada
[e] Institut für Geographie, University of Bremen, Germany
[f] Department of Earth and Ocean Sciences, University of British Columbia, Canada
[g] Department of Geosciences, University of Arkansas, USA
[h] Department of Geosciences and Geography, University of Helsinki, Finland
[i] Département des Sciences de la Terre et de l'Atmosphère, UQAM, Montréal, Canada

ARTICLE INFO

ABSTRACT

The Pingualuit Crater was formed by a meteoritic impact ca. 1.4 million years ago in northernmost Ungava (Canada). Due to its geographical position near the center of successive North American ice sheets and its favorable morphometry, the Pingualuit Crater Lake (water depth = 246 m) promises to yield a unique continuous sedimentary sequence covering several glacial/interglacial cycles in the terrestrial Canadian Arctic. In this paper, we suggest the existence of a subglacial lake at least during the Last Glacial Maximum (LGM) by hydraulic potential modeling using LGM ice-surface elevation and bed topography derived from a digital elevation model. These results support the hypothesis that the bottom sediments of the Crater Lake escaped glacial erosion and may contain a long-term continental sedimentary sequence. We also present the stratigraphy of a 9 m-long core retrieved from the deep basin of the lake as well as a multiproxy reconstruction of its deglacial and postglacial history. The base of the core is formed by very dense diamicton reflecting basal melt-out environments marking the end of subglacial conditions at the coring site. The overlying finely laminated silt are related to the onset of proglacial conditions characterized by extremely low lacustrine productivity. Infra Red Stimulated Luminescence and AMS ^{14}C dating, as well as biostratigraphic data indicate sediment mixing between recent (e.g. Holocene) and much older (pre- to mid-Wisconsinan) material reworked by glacier activity. This process prevents the precise dating of these sediments that we interpret as being deposited just before the final deglaciation of the lake. Two finer grained and organic-rich intervals reflect the inception of lacustrine productivity resulting from the cessation of glacial meltwater inputs and ice-free periods. The lower organic interval corresponds to the early postglacial period (6850−5750 cal BP) and marks the transition between proglacial and postglacial conditions during the Holocene Thermal Maximum, while the uppermost organic-rich core section represents late Holocene sediments (∼4200−600 cal BP). The organic intervals are separated by a basin-scale erosive slide occurring around 4200 cal BP and likely related to 1) a seismic event due to the glacio-isostatic rebound following the last deglaciation or 2) slope instabilities associated with rapid discharge events of the lake.

© 2011 Elsevier Ltd. All rights reserved.

1. Introduction

Current climatic changes are particularly intense and rapid in the Arctic region (e.g. Overpeck et al., 1997, 2006; Comiso, 2003; Perren et al., 2003; ACIA, 2004; Otto-Bliesner et al., 2006; Axford et al., 2009). In order to assess the environmental modifications in

* Corresponding author. Institut des sciences de la mer de Rimouski, Université du Québec à Rimouski, 310 allée des Ursulines, Rimouski, Québec G5L 3A1, Canada. Tel.: +1 418 723 1986x1230; fax: +1 418 724 1842.
E-mail address: herve.guyard@uqar.qc.ca (H. Guyard).

the Arctic over the last several decades, an understanding of the long-term fluctuations is important and can be achieved by identifying and studying terrestrial sites that preserved records of long-term environmental and climatic changes. Lake sediments in high-latitude regions are natural archives of climate and environmental variability because they contain records of past physical and chemical conditions as well as important biological indicators (Cohen, 2003; Pienitz et al., 2004). If long-term marine sedimentary records or glacial archives from Greenland are relatively well understood, there is almost no information available on climate dynamics in the terrestrial Arctic beyond the last deglaciation (e.g. ACIA, 2004; CAPE, 2006). Most of the lakes in the northern Hemisphere are of glacial origin or the sediments in the preexisting lakes were eroded by ice-sheet flow during past glaciations (Pienitz et al., 2008). Due to its location in close proximity to former centers of successive North American ice-sheets, where ice thickness was maximal and ice movement was minimal, and due to its particular shape and depth, the Pingualuit Crater Lake (61°17 N, 73°40 W; Ungava; Figs. 1, 2 and 3) may potentially yield a unique continuous long-term sedimentary sequence reflecting a succession of glacial/interglacial periods over the last 1.4 Ma in the terrestrial Canadian Arctic (Bouchard, 1989a). Physical and hydrological arguments suggested that the lake may have persisted under the flowing ice sheet (Bouchard, 1989b), supporting the idea that a subglacial lake existed at the center of the Laurentide Ice Sheet (LIS).

In northern Québec, the onset of deglaciation and the timing of the Holocene Thermal Maximum lagged behind other regions of the northwestern and northeastern Canadian Arctic (e.g. Kaufman et al., 2004; Kaplan and Wolfe, 2006). Due to the stagnant nature of the ice front on the rugged coastline, the LIS strongly influenced regional climate long after deglaciation was initiated around 12 ka cal BP along the southern shore of Hudson Strait and persisted until about 7.4 ka cal BP in northern Québec and Labrador (Lauriol and Gray, 1987; COHMAP, 1988; Saulnier-Talbot and Pienitz, 2009). According to Matthews (1963) and Lauriol and Gray (1987), the stationary nature of the ice front could be explained by local climate, characterized by cold humid summers and abundant snowfall in winter, allowing stabilization of the glacial front beyond 7.9 ka cal BP (Lauriol and Gray, 1987).

Until our study, only the upper 14 cm spanning the last 5030 ± 70 yr BP (5780 ± 135 cal BP) were sampled in Pingualuit Crater Lake (Bouchard et al., 1989a). Sediments are rich in pollen, diatoms and chironomids, thus promising for paleoenvironmental reconstructions (Richard et al., 1989; Gronlund et al., 1990). Here we present an AMS ^{14}C-based stratigraphy and a multiproxy paleoenvironmental reconstruction of a ~9 m-long sediment core retrieved in May 2007 from the deep basin of Pingualuit Crater Lake.

2. Study area

2.1. Origin, characteristics and age of the Pingualuit Crater

The Pingualuit meteoritic crater is located in the Ungava Peninsula, south of Hudson Strait about 80 km WSW of Kangiqsujuaq (Fig. 1), close to the area where the LIS reached its maximum thickness during the Wisconsinan glaciation (Bouchard and Marcotte, 1986; Marshall et al., 2000, 2002). Since deglaciation, this is also a climatologically sensitive location as the Hudson Strait connects the waters of the Canadian Arctic and Subarctic to the North Atlantic Ocean via the Labrador Sea. The Pingualuit Crater was formed ca. 1.4 million years ago, as determined by Ar/Ar dating of the impactites collected outside the crater (Grieve et al., 1991), and is classified as a simple crater (i.e. no central uplift and no inward collapse of the rim) (Bouchard and Marsan, 1989).

Today, the crater forms an almost perfect circular depression (Fig. 2) about 410 m deep and 3.4 km in diameter, hosting a unique purple-blue, clearwater ultraoligotrophic lake presently 246 m deep and 2.8 km in diameter (Gantner et al., submitted for publication). Pingualuit Crater Lake is one of the deepest and most transparent lakes (Secchi disc transparency in August 2011, = 33 m) on the planet (Ouellet et al., 1989; Gantner et al.,
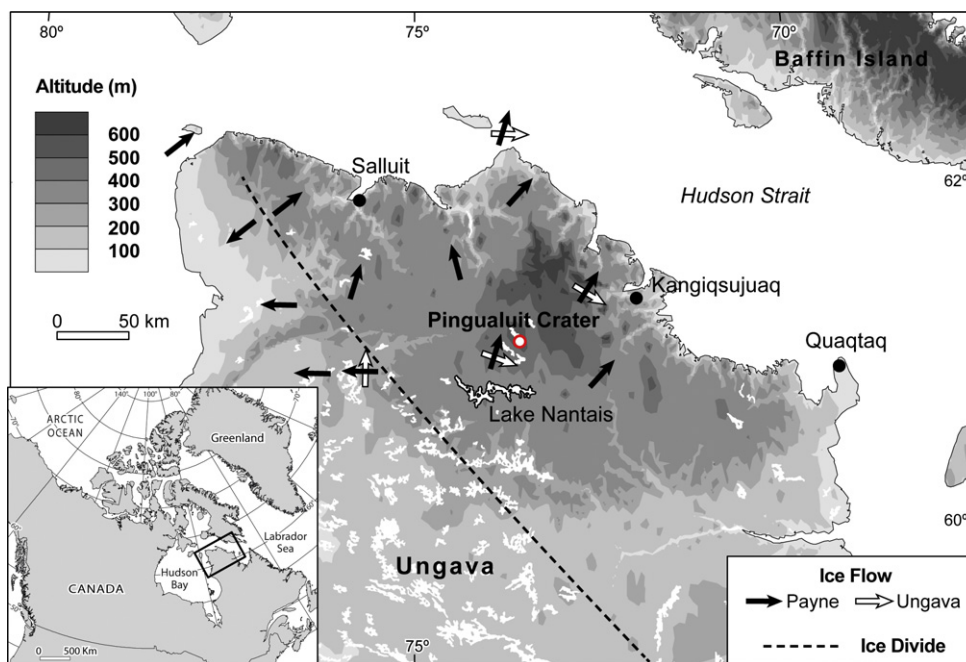

Fig. 1. Topographic map of northern Ungava and location of the Pingualuit Crater Lake (red circle). Also illustrated are the main ice flow directions (Ungava and Payne) deduced from accumulation and erosion forms (Bouchard and Marcotte, 1986; Daigneault and Bouchard, 2004) (arrows) and the ice divide line proposed by Daigneault and Bouchard (2004) (dashed line). (For interpretation of the references to colour in this figure legend, the reader is referred to the web version of this article.)
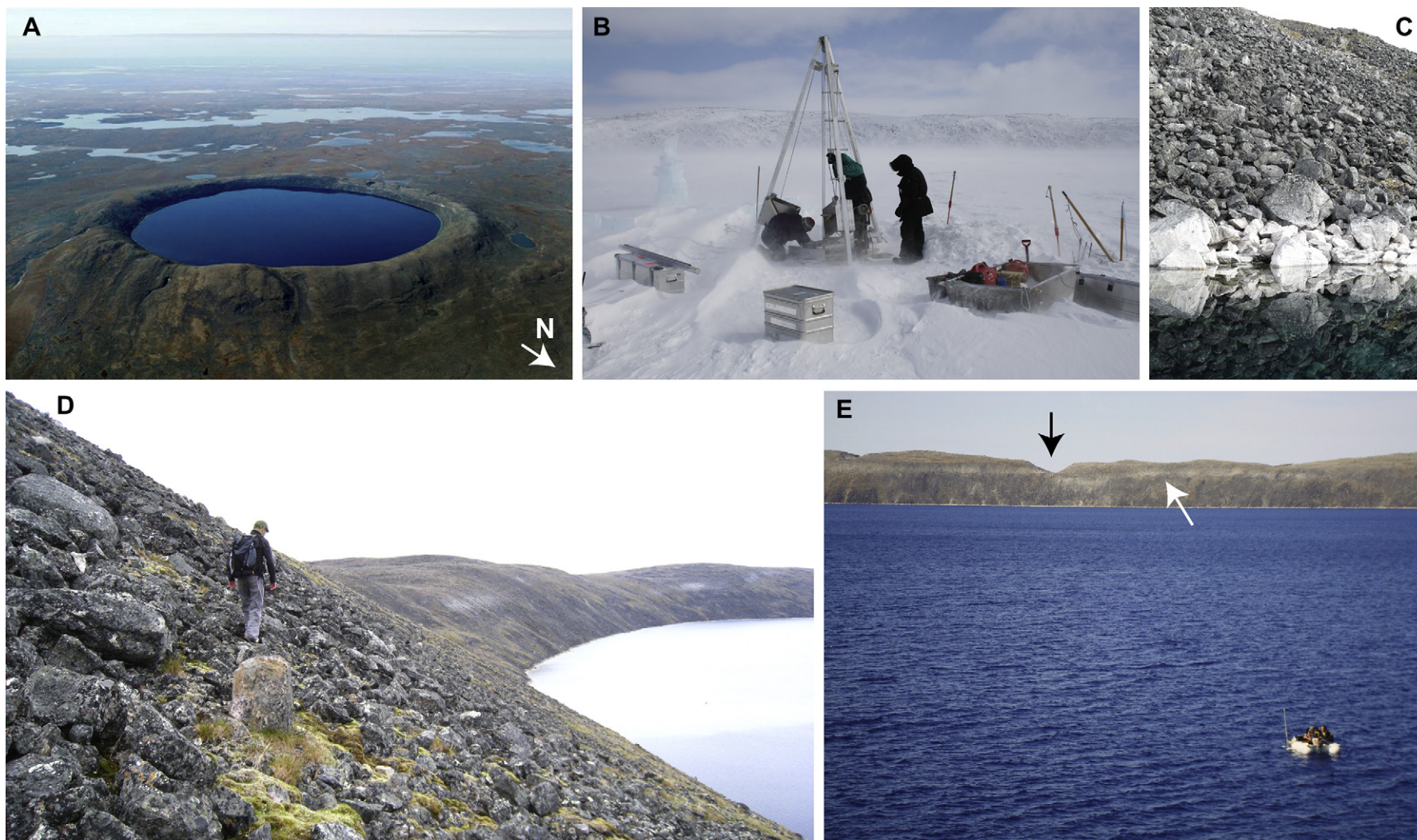
Fig. 2. Photographs illustrating (A) the isolated Pingualuit Crater Lake (photo: Robert Fréchette), (B) the UWITEC coring system used on the frozen lake surface, (C and D) the steep internal slopes composed of large blocks and lacking vegetation and soils (southern part of the crater on C and eastern part on D), and (E) one V-shaped discharge valley (some are also visible in A) and the associated 544 m a.s.l. paleo-shoreline (black and white arrows, respectively).
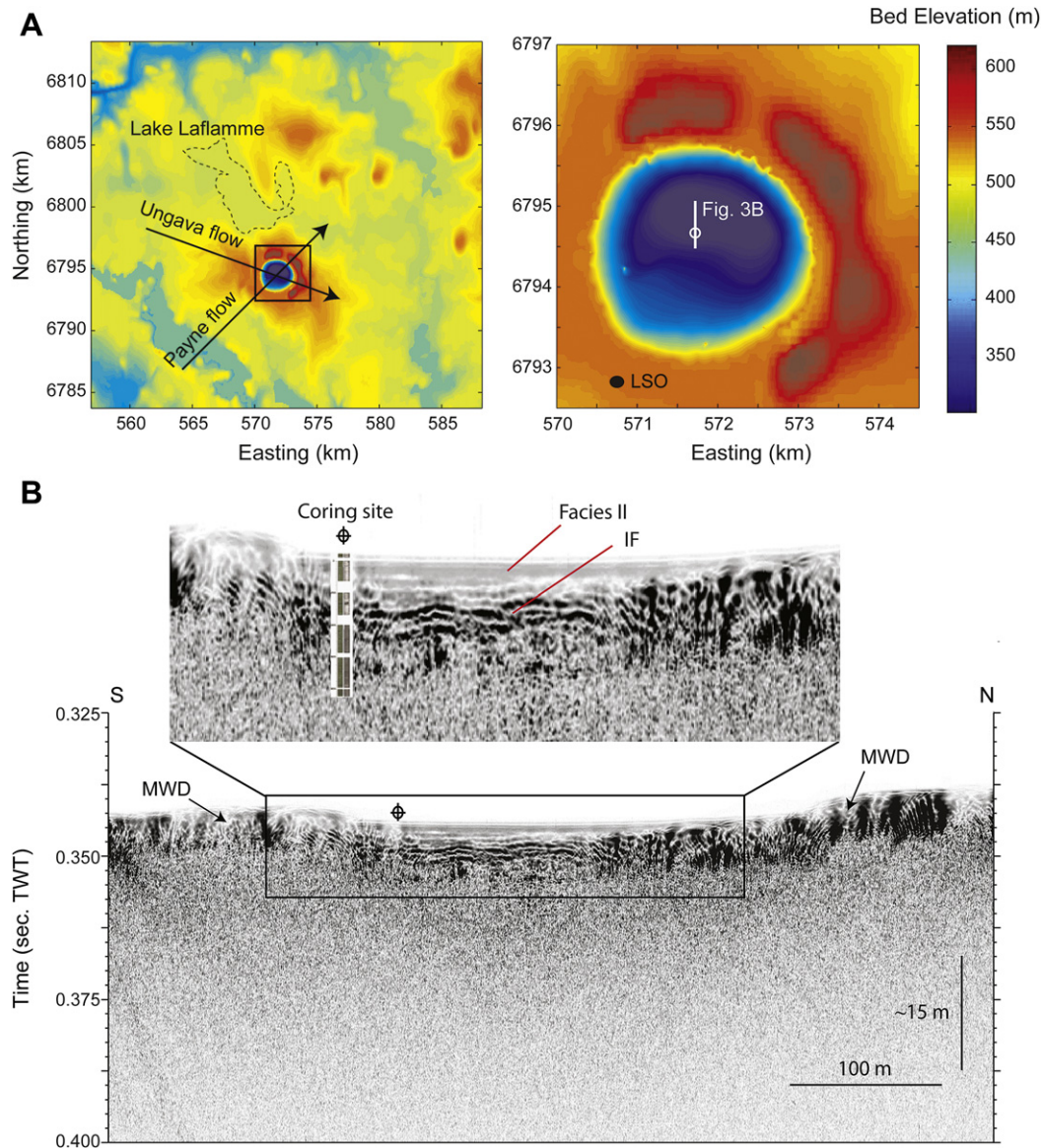
Fig. 3. (A) Bed topography (m) of the study area derived from a digital elevation model and main ice flow directions. Enlarged section on Pingualuit Crater Lake (right panel) and location of the coring site in the deep basin (244 m water depth; white circle). The white line indicates the position of the acoustic transect. The scale denotes bed elevations (m) and axes are in kilometers north and east. LSO: Lake du Sud-Ouest. (B) Acoustic profile at the coring site along a S–N direction obtained using a 3.5 kHz chirp during the August 2010 expedition. Vertical scale is in seconds (two way travel time). IF: inverse fault; MWD: mass wasting deposit.

submitted for publication) and has an extremely limited littoral zone due to its steep basin walls (26–35°) and boulder-strewn slopes (Fig. 2). The lake has no surface connection to other surrounding water bodies (Fig. 2) and is only fed with precipitation. Nevertheless, the existence of a cryptorheic drainage system (i.e. underground) between the Pingualuit Crater Lake and the neighboring Lake Laflamme (Fig. 3) is strongly suggested by $\delta^{18}O$ measurements of lake waters from both systems (Ouellet et al., 1989). The groundwater drainage probably occurs along a major and N–S oriented fault plan linking both lakes (Currie, 1965) and would explain the relatively stable level of the Crater Lake (at least over the last decades) despite a positive hydrologic balance. The residence time of the waters in the Crater Lake is estimated at around 330 years (Ouellet et al., 1989). The maximum altitude of the rim is 657 m a.s.l., which is one of the highest summits in Ungava (Fig. 1). It rises to 163 m above the present lake surface (494 m a.s.l) and 120 m above the surrounding terrain (Fig. 3).

2.2. Geological context

The study area lies on Archean bedrock dominated by granites and granitic gneisses (Currie, 1965). The exposed bedrock consists of a mixture of plutonic rocks of generally granitoid composition cut by occasional basic dykes. Low-grade hydrothermal mineralization and alteration is present on the inner wall of the crater and is believed to be related to the formation of the crater (Currie and Dence, 1963; Currie, 1965). Rocks of the rim are mineralized with epidote and hematite, and are altered to sericite. These minerals are not found in the same rock units outside the rim.

The landscape is covered with a 0–2 m-thick discontinuous veneer of till and boulders supporting very scarce tundra vegetation (Gray and Lauriol, 1985; Bouchard et al., 1989b; Daigneault and Bouchard, 2004). Mudboils, frost cracks, soil circles and stripes are the main frost features frequently observed on the till-covered surfaces. Glacial landforms in the study area are mostly

characterized by large erratic and perched blocks, but eskers and drumlins are also common (Bouchard et al., 1989b; Daigneault, 1997a,b).

2.3. Regional glacial history

The crater is situated at the center of successive Quaternary North American glaciations where ice movements and erosion were minimal (Dyke, 2004). Nevertheless, geomorphological features in the area surrounding the crater show at least two distinct regional glacial movements (Ungava and Payne flows; Figs. 1 and 3A) during the last glaciation (Gray and Lauriol, 1985; Bouchard and Marcotte, 1986; Lauriol and Gray, 1987; Bouchard et al., 1989b; Daigneault and Bouchard, 2004). Proterozoic erratic blocks derived from the North were recognized by Currie (1965) and thought to originate from the Ungava center, while all other ice flow indicators reveal that the subsequent flow was north-eastward, originating from the Payne center. The Ungava flow (oriented at the azimuth 110°; Fig. 3A) has preceded the Payne flow (oriented at the azimuth 45°; Fig. 3A), the latter being considered the main and sustained glacial flow of the last glaciation in the crater area (Bouchard et al., 1989b and citations therein). This ice flow produced loosely defined dispersal trains northeastward. Analysis of the fine fraction (<0.063 mm) of surface till samples (depth: 30 cm) in the Ungava Peninsula by Daigneault (2008) revealed anomalously high uranium content in the crater area, suggesting a regional dispersal train of U-rich material.

If some ephemeral glacial lakes (i.e. directly linked to the LIS retreat and blocked by the ice front) were formed during deglaciation in the Lake Nantais region (Taylor, 1982; Janssen, 2003), the water levels of such ice-dammed lakes are much lower than the minimum altitude of the crater (550 m). Because of the high altitude of the crater (representing the highest summit of the drainage basin, Fig. 3), it is very unlikely that the Pingualuit Crater Lake basin was invaded by any large regional glacial lakes (Bouchard and Saarnisto, 1989; Daigneault, 2008). The crater rim is also located too high to have allowed postglacial marine transgression in the lake, as the marine limit is estimated at 127 m a.s.l. near Kangiqsujuaq (Gray and Lauriol, 1985).

However, a temporary surface hydrological connection with neighboring Lake Laflamme (Fig. 3) just after deglaciation was proposed by Bouchard and Saarnisto (1989) to explain the presence of the single fish population in the Crater Lake, Arctic Char (*Salvelinus alpinus*) (Martin, 1955; Delisle and Roy, 1989; Gantner et al., submitted for publication). This hypothesis was based on the observation of one paleochannel connecting both lakes. The delta surface at the mouth of the channel indicates that the Lake Laflamme's level was at least 15 m above its present level. In summary, waters from glacial lakes have never drained in Pingualuit Crater Lake, which has only drained out during and just after deglaciation phases.

2.4. Regional deglaciation

Geomorphological features in the crater area suggest glacial retreat from the Hudson Strait coast toward the interior (i.e. from northeast to southwest) (Gray and Lauriol, 1985; Bouchard and Marcotte, 1986; Lauriol and Gray, 1987; Bouchard et al., 1989b; Bruneau and Gray, 1997; Daigneault and Bouchard, 2004). Deglaciation along the southern shore of Hudson Strait occurred between 12 ka cal BP and 7.8 ka cal BP (Gray and Lauriol, 1985; Lauriol and Gray, 1987; Gray, 2001; Saulnier-Talbot et al., 2009). Last remnants of the LIS persisted until *ca.* 7.4 ka cal BP in northern Québec and until 5.7 ka cal BP on Baffin Island where two ice caps remained

(Dyke and Prest, 1987). Lauriol and Gray (1987) proposed that the ice sheet persisted on the Ungava plateau until about 5.7 ka cal BP.

The transition between inorganic sedimentation and gyttja accumulation occurred between 7690 ± 260 cal BP and 7310 ± 310 cal BP in the Quaqtaq region (Richard, 1981) about 200 km ESE of Pingualuit Crater Lake (Fig. 1). Several radiocarbon dates on sedimentary humic acids recently obtained suggest that the coastal landscape was ice-free by 8065 ± 95 cal BP in the vicinity of Salluit (Fig. 1) and that the ice had started to retreat as early as 9630 ± 75 cal BP near Kangiqsujuaq (Saulnier-Talbot et al., 2009). Only a few studies have in fact dated lake sediment cores in the northern Ungava region (see review in Saulnier-Talbot et al., 2009). Bulk sediments of the base of the 14 cm-long grab sample previously recovered from the Pingualuit Crater Lake were dated at 5030 ± 70 yr BP (Bouchard et al., 1989a), corresponding to a calibrated age of 5780 ± 135 cal BP. The facies along with the fossil microflora, microfauna and the pollen content of the sediments (Richard et al., 1989; Grönlund et al., 1990) suggest that the lake was already ice-free at this time. According to Richard et al. (1989), these sediments would represent the entire postglacial period, while AMS ^{14}C dating of bulk sediments from Lake du Sud-Ouest (Richard et al., 1991), a small shallow lake located just outside the crater rim (Fig. 3A), places the transition between slightly organic clayey silt and silty gyttja at 7770 ± 160 cal BP.

Ten valleys, corresponding mostly to the faulting systems around the crater, can be observed at different altitudes crossing the rim (Currie, 1965; Bouchard and Marsan, 1989) and several of them connect to paleo-drainage channels formed during the last ice-sheet retreat (Bouchard and Marsan, 1989; Bouchard and Saarnisto, 1989). The successive rapid drainage events of the lake related to the deglaciation are indicated by three paleo-shorelines on the internal slopes of the crater reflecting successive lake level drops (Bouchard and Saarnisto, 1989). The highest paleo-shoreline (574 ± 5 m) is only detected on the northern half, while the well-developed paleo-shoreline around 544 ± 5 m (Fig. 2E) is visible all around the internal slopes of the crater. Finally, the lower paleo-shoreline (512 ± 3 m) is poorly developed but present all around the crater. The water drainage is also indicated by the washing of the till in the valleys and by their incised shape (Fig. 2E). When the crater was totally ice-free around 5780 ± 135 cal BP according to Bouchard et al. (1989a) and Richard et al. (1989), the lake maintained a postglacial surface connection with neighboring Lake Laflamme for an undetermined time. The connection may have persisted as long as the Crater Lake level was at 550 m a.s.l. (Bouchard and Saarnisto, 1989). Due to the significant depth of the lake, the possibility that lake bottom sediments escaped the crater during these rapid drainage events is negligible. The sediments that accumulated in the Pingualuit Crater Lake basin since its formation therefore remained *in situ* and intact (Bouchard, 1989a).

2.5. Sedimentation within the Pingualuit Crater Lake

Today, the crater acts as a large natural atmospheric precipitation collector and as a closed sedimentary basin (Fig. 2). This situation has probably persisted during ice-free periods since 1.4 Ma. The basin is asymmetric with a plateau (situated in the south-southwestern part of the lake) and a deeper basin (situated in the northwestern part of the lake) (Fig. 3A). Currie (1965) initially believed that the deep basin resulted from more intense glacial erosion, but seismic studies revealed that more sediment has accumulated on the plateau than in the deep basin (Moussawi and Tessier, 1989). This asymmetry may be explained by an intense sedimentation episode during the last deglaciation (Bouchard, 1989a). Most of the lake sediments contain blocks/boulders, except for the upper 25 m in the deep basin where

sediments are finer in grain size (Moussawi and Tessier, 1989). According to these authors, the upper 25 m do not show any signs of diffraction indicating finer sediments, while the sequence below (between 25 and 70 m) is characterized by chaotic seismic structures, revealing the presence of larger clasts. A deeper reflector was detected at around 90 m below the lake floor (blf). However there is no evidence that this reflector corresponds to the base of the sedimentary pile and the roof of the impact breccia. An accumulation of a minimum of 90 m of sediments is therefore likely in the deep part of the basin (Moussawi and Tessier, 1989). The main results obtained from Moussawi and Tessier (1989), together with detailed acoustic data recently collected will be discussed elsewhere. Whereas sediments covering the plateau (55–73 m thick) result from the last deglaciation associated with subglacial melt-out deposits, sediments in the deepest basin probably represent prolonged cumulative subglacial sedimentation (Moussawi and Tessier, 1989; Bouchard, 1989a). In other similar settings (e.g. Lake El'gygytgyn; Niessen et al., 2007), turbidites triggered in the littoral zones or on the slopes of the lake travel over long distance, and distal turbidites are clearly visible. Likewise, distal turbidites may also be visible in the deep basin of Pingualuit Crater Lake.

3. Materials and methods

3.1. Acoustic profiling and sediment coring

The Pingualuit Crater Lake is the most important feature of the Pingualuit National Park and is managed as an extremely protected area (MDDEP, 2005). The coring site was selected according to the previous seismic study of Moussawi and Tessier (1989) which identified a sediment accumulation of at least 90 m in the deep basin using a boomer Geopulse 5813A (384 Hz) source and 12 hydrophones. At the coring site in 2007 (61°N 16′46.5″; 73°W 39′44.7″; 244 m water depth; Fig. 3), a hole for the coring system (equipped with basal plate and reentry cone) was cut through the ice. Using both the UWITEC gravity and percussion piston coring systems from the frozen surface of the lake (Fig. 2), the uppermost ~9 m of sediments were recovered in May 2007 under harsh weather conditions and subject to strict environmental regulations. As such, only one hole was allowed for the coring and therefore core recovery between sections is incomplete (Figs. 4 and 5). Coring operations were stopped around 8.5 m below the lake floor upon reaching a diamicton layer impermeable to the coring device. All the core sections were placed in specifically designed heated boxes to prevent them from freezing.

In August 2010, a more detailed acoustic survey using a 3.5 kHz sub-bottom profiler (Knudsen Chirp 3212) allowed the study of the sediment architecture and basin morphology (Ledoux et al., 2011). This acoustic survey was once again performed under the strictest possible environmental regulations to avoid any contamination of the pristine lake waters by gasoline or external/exotic biota. All equipment in contact with water was washed in the field and all scientific instruments were powered by electrical batteries that were recharged daily outside the crater rim. To compute a first order sediment depth scale from the acoustic travel times, we conservatively assumed the sound velocity in the water column to be 1420 m s^{-1} (Moussawi and Tessier, 1989) and in the saturated sediments to be 1500 m s^{-1} (Fig. 3). The apparent weak penetration of the signal (ca. 10 m; Fig. 3B) is due to the presence of coarse-grained sediments and to the type of device used, as a higher energy seismic source was not allowed. As a consequence of this weak penetration, the signal obtained does not represent the entire sedimentary sequence (see section 2.5).

3.2. Multiproxy analysis of the sediment cores

In the laboratory, the core sections were first run through a Multi Sensor Core Logger to measure volumetric magnetic susceptibility and wet bulk density by gamma ray attenuation at 1 cm intervals calibrated according to a procedure described in St-Onge et al. (2007). The cores were then split, described and photographed using a 500 d.p.i. resolution digital camera, and diffuse spectral reflectance (sediment color) was measured at 1 cm intervals using a hand-held spectrophotometer. Data were converted into the CIE (Commission Internationale de l'Éclairage/International Commission on Illumination) L* a* b* (L*: lightness; a*: from green to red; b*: from blue to yellow) color space. Magnetic susceptibility was further refined with a point sensor on the split core sections at 0.5 cm intervals. These data are presented here.

U-channels were then sampled in the center of the short gravity and long piston cores for subsequent very high-resolution physical and geochemical analyses (CAT-Scan and micro XRF core scanner analyses) in undisturbed sediments. CAT-Scan (computerized axial tomography) analyses were carried out a first time on half sections at the Hôpital Régional Rimouski with a pixel resolution of 3 mm. Analyses were then refined on u-channels at INRS-ETE (Québec City) with a pixel resolution of 0.1 mm. This non-destructive tool allows quantification and mapping of X-ray attenuation coefficients of the sediment cores on longitudinal images (topograms). Data were processed with the Igor software according to St-Onge and Long (2009). The resulting images are displayed in greyscale with the darker grey representing lower X-ray attenuation and lower bulk density values (e.g. Guyard et al., 2007; St-Onge et al., 2007).

Micro-fluorescence-X (XRF) analyses were completed at INRS-ETE with an ITRAX core scanner (e.g. Croudace et al., 2006; Guyard et al., 2007; St-Onge et al., 2007) at a downcore resolution of 200 μm for most of the sections, and at 100 μm for intervals of special interest (i.e. organic intervals). The ITRAX core scanner uses an intense non-destructive micro X-ray beam that irradiates the sample (duration 30 s for the intervals of interest and 10 s for the rest of the core) to collect positive X-radiograph images and to detect the energy of fluorescent radiation to provide high-resolution relative concentrations of elemental profiles (from Al to U) (e.g. Croudace et al., 2006; Francus et al., 2009). The ITRAX X-radiograph images are 2 cm wide with a pixel size of 0.1 mm, while XRF analyses are measured from a 4 mm-wide and 0.1 mm-thick area.

Total carbon (TC) was measured on 227 dried, crushed and homogenized samples at variable intervals using a CNS elemental analyser (EuroEA, Eurovector) at Bremen University. Thereafter, a subset of 10 pilot samples was treated successively with 3% and 20% hydrochloric acid at 80 °C to remove the carbonates. By re-measuring these samples with the CNS elemental analyser, total organic carbon (TOC) was determined. Total inorganic carbon (TIC) was then calculated as the difference between TC and TOC. As the TIC record is very low (<0.1%; mean = 0.013%, $n = 10$) and more or less fluctuates around zero, these values are realistically not taken into consideration for the interpretation. As such, the TC record is regarded and reported as being identical to TOC. This is also supported by the fact that no carbonates are present in the watershed (Bruneau and Gray, 1997; Daigneault and Bouchard, 2004). The δ^{13}C content of the sedimentary organic matter were determined at GEOTOP on dried, ground and acidified aliquots using a Micromass Isoprime mass spectrophotometer. For the determination of biogenic silica (BSi), 20 selected samples were digested with a sodium hydroxide solution to dissolve the diatom frustules. The BSi was then measured photometrically according to the method developed by Müller and Schneider (1993) using continuous-flow-analysis.
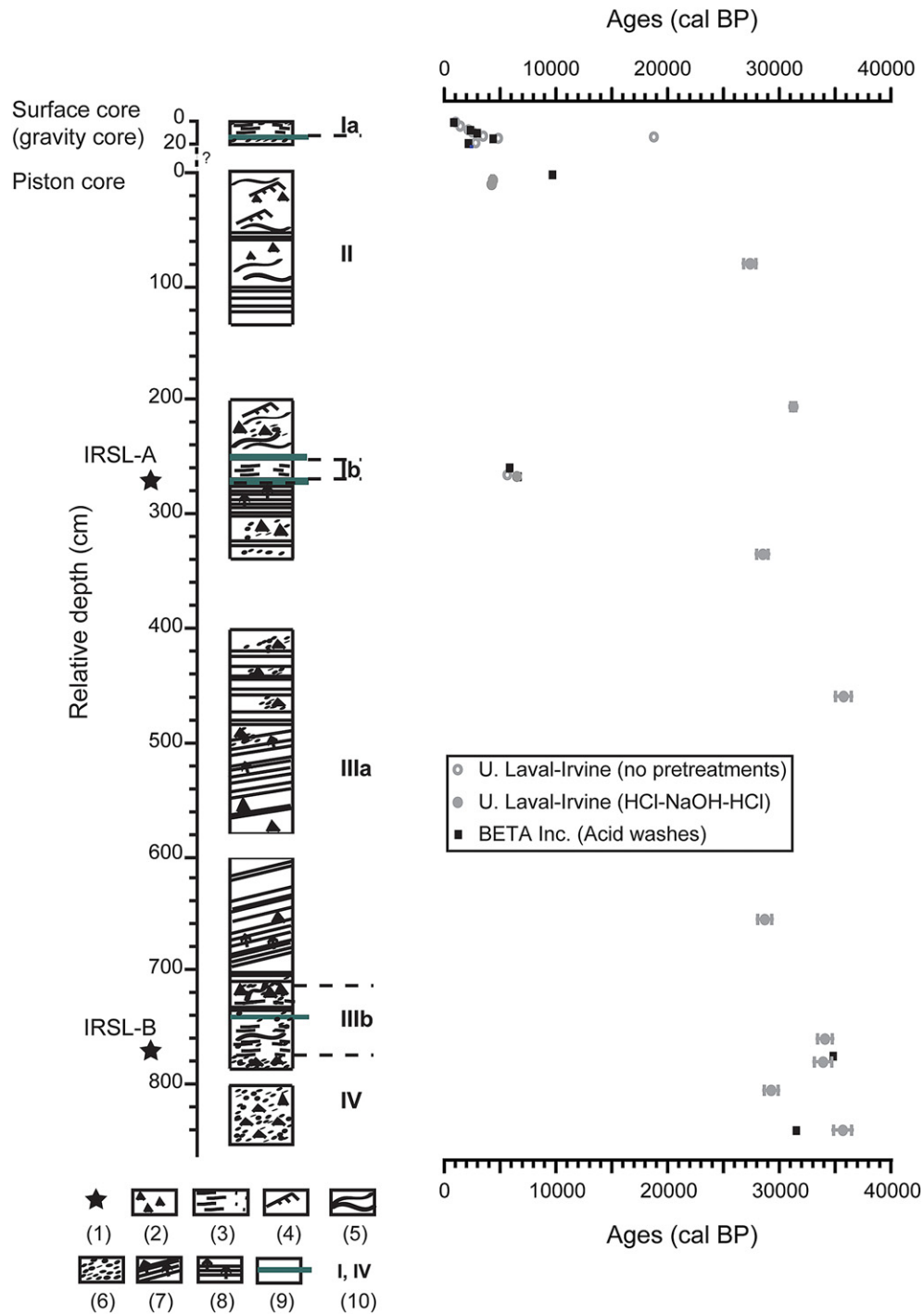
Fig. 4. General simplified stratigraphy of the cores. Also illustrated (right graph) are the calibrated ^{14}C dates obtained from two distinct laboratories (cal BP) as well as: (1) Location of IRSL samples (IRSL-A: ∼70 ± 14 ka; IRSL-B: sediment not zeroed; see section 3.3.2), (2) Angular lithified cm-scale clasts (dropstones), (3) Organic-rich clayey silt, (4) Cross-laminations, (5) Large folds and deformations, (6) Muddy sand intervals, (7) Inclined and normal graded laminations in inorganic sandy silt intervals, (8) Horizontal and normal graded laminations in inorganic sandy silt intervals, (9) Compact, light clay layer. (10) Facies numbers discussed in the text.

3.3. Chronology

3.3.1. AMS [14]C

The absence of datable macrofossils or plant remains in sediment cores from Arctic lacustrine environments constitutes a major challenge for the establishment of reliable chronologies (Abbott and Stafford, 1996; Wolfe et al., 2004). Accelerator mass spectrometry (AMS) radiocarbon dating of bulk sediments was thus

used to assess the age-depth relationship in the cores from the Pingualuit Crater Lake. All samples sent to Beta Analytic Inc. (Florida, USA) were washed by an acid solution, while several samples sent to Université Laval (Québec City, Canada) for the preparation of the gas (using the method described by Abbott and Stafford, 1996), then to the University of California Irvine for the radiocarbon measurements were not pretreated (cf. Table 1) because of the low sediment availability. In high-latitude environments, slow

Table 1
^{14}C and IRSL dating on bulk sediments from the surface and piston cores of the Pingualuit Crater Lake.

Facies #	Lab no. (dating)	Lab no. (gas extraction)	Pretreatments	Relative depth (cm)	Conv. age (^{14}C yr BP)[d]	±	Calib. age (2σ) (cal BP)	±
	Surface core							
Ia	Beta-256021[a]		Acid washes	0–1	830	40	740	60
Ia	UCI-47806[b]	ULA-620[c]	None	0.4–0.7	1110	20	1010	45
Ia	Beta-256022		Acid washes	4–4.7	1510	40	1420	100
Ia	UCI-47807	ULA-621	None	4.2–4.5	1520	20	1430	80
Ia	Beta-256023		Acid washes	6.7–7.7	2310	40	2265	105
Ia	UCI-47803	ULA-617	None	7.4–7.7	2150	20	2180	120
Ia	Beta-256024		Acid washes	10.3–10.8	2920	40	3080	130
Ia	UCI-47808	ULA-622	None	10.4–10.7	2430	20	2520	160
Ia	UCI-47809	ULA-623	None	13.1–13.3	3255	20	3485	75
II	UCI-47810	ULA-624	None	13.6–13.9	15560	60	18750	140
II	Beta-256025		Acid washes	14.5–15.7	4320	40	4905	65
II	UCI-47811	ULA-625	None	14.6–14.9	4255	20	4840	14
Ia?	UCI-47812	ULA-626	None	17.3–17.6	1885	20	1810	70
Ia?	Beta-256026		Acid washes	18.3–19.3	2120	40	2150	160
Ia?	UCI-47813	ULA-627	None	18.8–19.1	2725	20	2820	44
	Piston core							
II	Beta-256027		Acid washes	0–2	8680	50	9660	120
II	UCI-74434	ULA-1549	HCl–NaOH–HCl	5	3885	15	4330	80
II	UCI-75730	ULA-1550	HCl–NaOH–HCl	10	3825	15	4220	70
II	UCI-76678	ULA-1628	HCl–NaOH–HCl	78.5–80	22660	130	27365	535
II	UCI76679	ULA-1629	HCl–NaOH–HCl	204.5–205.5	26870	220	31265	245
Ib	Beta-256019		Acid washes	257.5–258.5	5080	40	5825	95
Ib	UCI-47802	ULA-616	None	264.8–265.2	4895	20	5625	28
Ib	Beta-256020		Acid washes	265.5–267.5	5800	40	6585	85
Ib	UCI-49080	ULA-655	HCl–NaOH–HCl	266–267	5705	25	6485	75
IIIa	UCI-76680	ULA-1630	HCl–NaOH–HCl	334–335	23730	150	28510	510
IIIa	UCI77051	ULA-1631	HCl–NaOH–HCl	459–460	31200	320	35740	710
IIIa	UCI77054	ULA-1632	HCl–NaOH–HCl	654.5–655.5	23870	250	28715	625
IIIb	UCI-75736	ULA-1551	HCl–NaOH–HCl	760	29550	270	34085	655
IIIb	Beta-275124		Acid washes	775	30060	260	34785	365
IIIb/IV	UCI-75731	ULA-1552	HCl–NaOH–HCl	780	29310	330	33915	750
IV	UCI-75737	ULA-1553	HCl–NaOH–HCl	805	24570	170	29280	630
IV	Beta-275125		Acid washes	840	27760	210	31485	325
IV	UCI-75732	ULA-1554	HCl–NaOH–HCl	840	31080	420	35670	810
	IRSL dating[e]						Age	±
Ib	IRSL-A			268–272			70000	14000
IIIb	IRSL-B			762–764			NZ	

[a] BETA = Beta Analytic Inc.
[b] UCI = University of California Irvine.
[c] ULA = Université Laval.
[d] Conventional age is the δ^{13}C-corrected AMS ^{14}C measurement that is used for all subsequent calibrated ages.
[e] IRSL-A: mean between estimated ages of coarse grained and fine-grained feldspars. NZ = sediment not zeroed. See section 3.3.2.

catchment processes (e.g. limited plant decomposition and soil development) can sequester organic matter for prolonged periods of time before it becomes incorporated into the lake sediment archive (Wolfe et al., 2004; Saulnier-Talbot et al., 2009). However, because the Pingualuit Crater has no tributary and no soil on its rim or shelf (Fig. 2), no lag effect is expected in organic intervals deposited in ice-free conditions as the organic matter is believed to derive exclusively from lacustrine productivity. Because untreated samples generally yield younger ages than treated samples as the acid treatment removes the possible recent contamination, and because we obtained more treated dates, our interpretation is preferentially based on the latter. Radiocarbon ages were corrected for isotopic fractionation and reported at a δ^{13}C value of −25‰. These conventional ages were then calibrated (Table 1) using the CALIB 6.0 software (Stuiver et al., 2010).

3.3.2. Infra Red Stimulated Luminescence (IRSL)

Two samples were selected to be dated by Infra Red Stimulated Luminescence (IRSL), one in the organic-rich sediment unit of the piston core (IRSL-A: relative depth = 268–272 cm) and one in the lower part of the core (IRSL-B: relative depth = 762–764 cm) (see Fig. 4). The IRSL measurements follow the standard luminescence protocol applied to feldspar as developed in the Montréal laboratory and described by Lamothe (2004).

The single aliquot regeneration (SAR) method applied to feldspar involves measurements of IRSL following a cut heat at 280 °C. A further and similar cut heat followed by a shine down of 60 s is inserted between the luminescence measurement following the natural or laboratory regenerated dose (e.g. Ln and Lx) and the luminescence measurement of the test dose (Tn and Tx). Several aliquots from different grain size fractions (e.g. 4–11 μm and 62–88 μm) were measured for both samples. The fading measurement followed the routine described by Auclair et al. (2003). The anomalous fading rate (termed g) value measurement for these samples is somewhat scattered but an average value of 7% can be assessed for both samples. The annual dose was estimated from instrumental neutron activation analysis (INAA) and thick source alpha counting of several core samples. As the sediment analysis yielded significant levels of U and Th, several sediment samples have been reanalyzed and one sample was further investigated to detect eventual disequilibrium by alpha spectrometry. For the environmental dosage we used a U content of 9.3 (±0.9) ppm, a Th content of 28.1 (±1.7) ppm and a K content of 2.12 (±0.7) %. Cosmic contribution was considered insignificant. A value of 12.5% of internal K was used for the dose rate to the coarser grain size. The assessment of the water content was based on *in situ* and laboratory analysis, as well as from the gamma density parameters. The water content was assumed to have been 75% for the whole geological
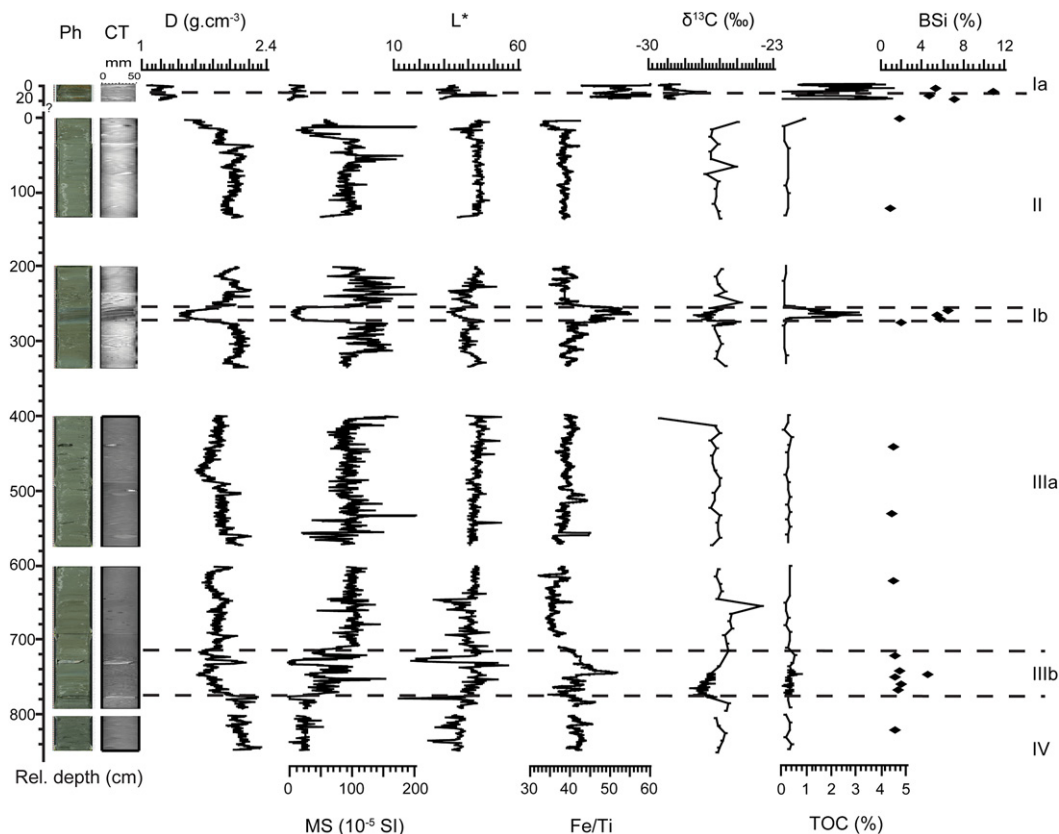
Fig. 5. High-resolution geochemical, physical and magnetic properties of the sediments. Facies numbers are also reported. Ph: Digital photographs of the cores; CT: topograms obtained from CAT-Scan analysis; D: wet bulk density; MS: volumetric magnetic susceptibility; L* is lightness according to the CIE Lab color space; Fe/Ti as measured by the ITRAX core scanner and smoothed over 100 points; TOC (%): total organic carbon; BSi (%): biogenic silica.

period. The annual dose obtained for the younger sample IRSL-A is around 4.5 ($\pm$0.4) Gy-ka^{-1} for the coarser fraction and 5.7 ($\pm$0.6) Gy-ka^{-1} for the fine grains. The lower sample, albeit undatable, was found to be in excess of 7 Gy-ka^{-1}.

The ages were calculated using the dose rate correction (DRC) method introduced by Lamothe et al. (2003). Therein, the equivalent dose measured is corrected for anomalous fading (AF) using an equation for which the most important parameters are the anomalous fading rate and the ratio between the laboratory and the environmental dose rate. The corrected equivalent dose, termed paleodose, divided by the annual dose yields the AF-corrected IRSL age. The AF-corrected natural luminescence of the lower sample, IRSL-B from 762 to 764 cm, suggests dose saturation, typical of feldspar grains that would have never been exposed to sunlight. In the case of the upper sample, IRSL-A from 268 to 272 cm, the IRSL properties of the aliquots used for measurements suggest bleaching by sunlight prior to final deposition. The coarse grained feldspars yielded a combined age of 74 ka ($\pm$9 ka) whereas the fine grains suggest an age of 66 ka ($\pm$10 ka). When the ages obtained represent overestimations for the timing of the depositional events, they should be considered as apparent.

3.4. Hydraulic potential modeling

To assess the likelihood that the crater provided a site for a subglacial lake we computed hydraulic potentials (e.g. Clarke, 2005, p252) at the base of the ice-sheet using Last Glacial Maximum (LGM) ice-surface elevation and bed topography derived from a digital elevation model (DEM) isostatically adjusted proportionately to the ice thickness (Marshall et al., 2000, 2002; Peltier, 2002).

Ice-surface in the region of interest was approximated by a planar surface inclined in the direction of inferred ice flow. Basal ice was assumed to be at the melting temperature so that the flow of subglacial water was not impeded by thermal barriers.

The potential energy of water depends on its elevation and pressure. The water pressure at the base of an ice sheet tends to be very close to the ice flotation pressure. We assume both are equivalent so that the downward force associated with ice overburden is exactly matched by an upward force associated with lake water pressure. Here we express hydraulic potential (Pa) in terms of hydraulic head (m) so that results can be plotted on the same graph as those depicting topographic elevations.

We estimate the extent of the subglacial lake by making the reasonable assumptions that the ceiling ice is floating on the lake and that hydraulic potential is exactly constant in the lake. The hydraulic potential in the lake contains contribution from the gravitational potential energy owing to the elevation of water in the lake, from ice overburden pressure to water pressure in the lake and from the added water pressure from the overlying water. We delineate the elevation of the lake ceiling by assuming that the lake is brimful. For a subaerial lake this would imply that the basin of the lake was filled to the elevation of the lowest spillway determined by the bed surface topography $z_b(x,y)$ where x and y are map position coordinates. For a subglacial lake the situation is analogous but it is the topography of the hydraulic head $h(x,y)$ that controls the location of spillways. Unlike subaerial lakes, the upper boundary of subglacial lakes need not be horizontal or flat.

To determine the brimful level of the basin we adopt a standard procedure of DEM analysis termed *pitfilling* which, in effect, replaces the void volumes contained within closed depressions by solid

material. The filling level is progressively increased until a topographic spillway is encountered. The method is commonly used in conjunction with drainage routing algorithms in order to remove water-trapping "pits" from a DEM. By applying this method to the DEM of hydraulic head we establish the maximum filling level for the subglacial lake. By assuming the lake is brimful, we implicitly assume that the subglacial bed is wet and that water is free to enter and exit the lake by flowing along the bed. This contrasts with the situation in subglacial Lake Vostok where the water level is largely controlled by thermal processes operating at the ice ceiling.

The source digital data of the Canadian Digital Elevation Data at the scale of 1:50 000 was extracted from the hypsographic and hydrographic elements of the National Topographic Data Base, while bathymetric data were obtained from Bouchard and Marsan (1989). The model was implemented within the MATLAB® programming environment using the DEM pit-filling algorithm developed by Soille and Gratin (1994).

4. Coring site and general stratigraphy of the core

4.1. Acoustic profile at the coring site

Acoustic profiles along the S-N axis of the lake indicate very steep slopes on both sides of the lake with mass wasting deposits at their foot, as reflected by chaotic and transparent reflections (Fig. 3B; Ledoux et al., 2011;). The steep slopes are also evident in the field (Fig. 2C and D). These typical acoustic facies dominate the lake bottom. Some discontinuous high amplitude reflections are only detected in the deep basin and indicate around 7.5 m of acoustically-stratified sediments. The presence of an inverse fault throughout the high amplitude reflections (Fig. 3B) suggests that these fine-grained sediments have been disturbed by post-depositional processes due to mass wasting probably originating from the particularly steep northern slope of the crater (Fig. 3). The upper part of the acoustic profile represents a 2–3-m thick transparent and low amplitude acoustic facies that covers the entire deep basin and corresponds to the sedimentary facies II (Fig. 3B, see below).

4.2. Lithofacies and physical properties of the sediments

Most of the sediments retrieved in the deep basin consist of relatively dense light grey sandy silt containing several angular rock fragments, and are characterized by very low organic carbon ($<0.3\%$; $n = 123$) and biogenic silica (1.7%; $n = 13$) contents (Facies IV, III, II; Figs. 4 and 5). In these facies, $\delta^{13}C$ values show a more pronounced variability and reached values $> -24\%$ (Fig. 5). Two decimeter-thick darker and finer intervals (Facies Ib and Ia) are sharply contrasting with these facies and are characterized by higher organic carbon ($>2\%$; $n = 57$) and biogenic silica (6.8%; $n = 5$) contents, and relatively lower density, magnetic susceptibility and $\delta^{13}C$ values (Figs. 4 and 5).

Facies IV (849–780 cm) is characterized by very dense and dark sediments as recorded by the lower L* values (e.g. St-Onge et al., 2007). TOC (0.27%; $n = 7$) and BSi (1.3%; $n = 1$) contents and magnetic susceptibility values are very low (Fig. 5). $\delta^{13}C$ values are relatively high ($>-25.9\%$; $n = 8$). This heterogeneous unsorted sandy mud interval also contains several cm-scale angular rock fragments (Fig. 4).

Facies III (780–270 cm) is characterized by less dense and lighter sediments with higher magnetic susceptibility values. From 780 to 710 cm (Facies IIIb), L*, Fe/Ti and magnetic susceptibility values increase, while density decreases. Sediments are faintly laminated, finer and soupy (Fig. 5). TOC ($>0.33\%$; $n = 67$) and BSi ($>2.1\%$; $n = 6$) contents are slightly higher and reach values up to

0.76% and 4%, respectively (Fig. 5). $\delta^{13}C$ values are slightly lower ($<-26.7\%$; $n = 60$). This deformed interval is intercalated between two rock fragments as large as the inner diameter of the liner tube (6.4 cm) and embedded in a sandy mud matrix (Figs. 4 and 5). Sediments between 710 and 270 cm (Facies IIIa) generally consist of finely laminated ($<1-2$ mm) silt (rhythmites) containing a few dropstones and/or sandy layers (Figs. 4 and 5). TOC ($<0.25\%$; $n = 48$) and BSi ($<1.4\%$; $n = 4$) contents are very low. $\delta^{13}C$ values are relatively high ($>-26\%$; $n = 49$). Laminations are oblique at the base and then become more horizontal upwards. The Fe/Ti ratio slightly increases up to 270 cm blf (Fig. 5).

Facies Ib (270–257 cm) consists of a decimeter-thick, organic-rich (1.8%; $n = 22$) clayey silt interval characterized by much lower density (also shown by CT-Scan and X-ray images), $\delta^{13}C$ ($<-26.7\%$; $n = 24$) and magnetic susceptibility values, and containing more BSi (5.9%; $n = 3$). Fe/Ti ratio values are much higher than in the rest of the core (Fig. 5). The transition between finely laminated silt (Facies IIIa) and facies Ib is marked by a 3-cm thick blue compact clay layer between 273 and 270 cm (Figs. 4 and 5).

Facies II (257–0 cm blf) is found at the top of the piston core and consists of deformed sediments yielding the same physical properties as facies IIIa (i.e. high density and magnetic susceptibility values, low TOC and BSi contents, relatively high $\delta^{13}C$ values and lower Fe/Ti values; Figs. 4 and 5). CT-Scan and X-ray images in facies II show folded structures, cross and horizontal laminations. Its base (257–255 cm blf), characterized by an erosive contact as revealed by the CT-Scan images and sharp variations in the different proxies, is associated with a thin compact blue clay layer (Figs. 4 and 5). Facies II can be identified in the seismic profile as a low amplitude and transparent facies (Fig. 3B) and is intercalated between facies Ib and facies Ia, the latter being located in the surface core.

No correlation was possible between the short gravity and the long piston core using the different proxies, likely indicating a small but undetermined sediment gap between both cores (Figs. 4 and 5). The last 3 cm of the surface core (17–20 cm) are defined by disturbed organic sediments (Fig. 4 and Table 1). Between 17 and 14.5 cm, very dense and inorganic sediments with high values of Fe/Ti ratio are observed. A blue, compact, inorganic clay layer is observed between 14.5 and 13.5 cm. Facies Ia is an organic-rich interval (13.5–0 cm) yielding similar characteristics than facies Ib (Fig. 5). BSi (8%; $n = 2$) and TOC ($>2.2\%$; $n = 35$) values are slightly higher than in facies Ib. $\delta^{13}C$ values in facies Ia are the lowest ($<-28.4\%$; $n = 35$) measured throughout the core. Finally, a thin sand layer between 1.5 and 3 cm is observed in the surface core and characterized by lower TOC and higher density values.

5. Core chronology and paleoenvironmental history

5.1. Existence of a subglacial lake

Results of the hydraulic potential modeling (Fig. 6) at the base of the ice sheet confirm the possibility that the crater basin hosted a subglacial lake during the LGM. Subglacial meltwater flow is driven by gradients of the hydraulic potential surface, and water should pond to accumulate as a subglacial lake in locations of local minima in this surface. The high fluid pressures modeled at the rock/ice interface around the basin combined with the depression morphometry thus suggest storage of subglacial water within the crater. The water being incompressible, the ice penetration in the basin was limited by the water evacuation throughout the crater's inner walls. If the current cryptorheic drainage beneath the crater toward Lake Laflamme had persisted during glacial periods, the underground drainage system should have been more distal and
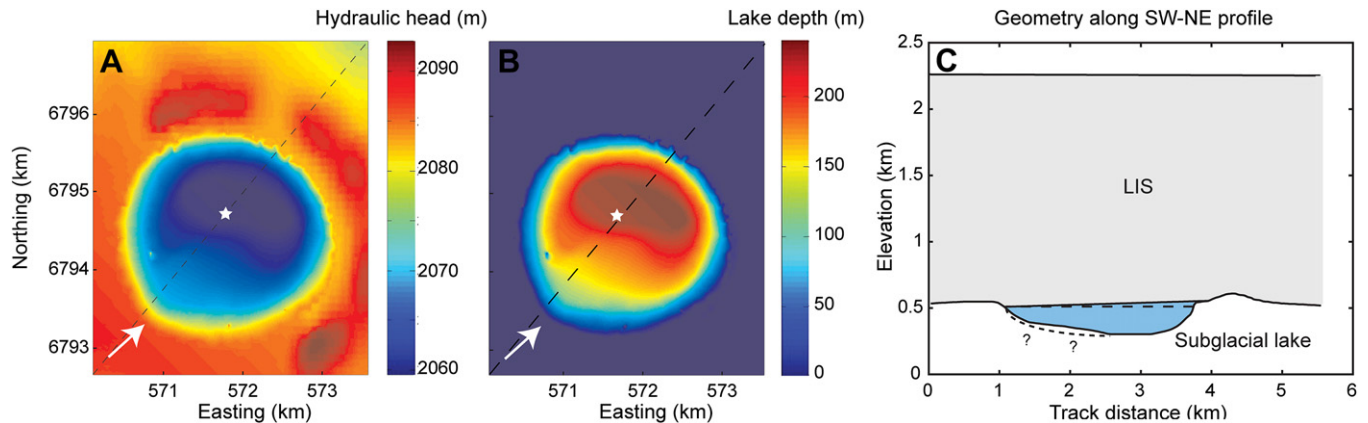
Fig. 6. Hydraulic potential modeling results for the Last Glacial Maximum (LGM; 20 ka) following the main ice flow direction (illustrated by arrows; Bouchard and Marcotte, 1986; Daigneault and Bouchard, 2004) and considering a 1700 m ice thickness (Dyke et al., 2002; Marshall et al., 2002) and a mean ice sheet slope of 0.1°. (A) Hydraulic head (m) for the Pingualuit Crater. (B) Pingualuit subglacial lake depth (m). (C) Geometry along SW-NE profile (illustrated by dashed lines on Fig. 6A and B). Note that the lake surface slope is in the opposite direction from the ice-surface slope. LIS: Laurentide Ice Sheet.

much reduced as the Lake Laflamme basin was occupied by an ice cap. Consequently, the entering rate of the ice in the basin would have been strongly restricted. Geothermal melting of any entering ice during its downward vertical progression may also have contributed to the persistence of the subglacial lake. The model simulations reveal that the geometry of the subglacial lake is independent of the ice thickness but highly influenced by the magnitude and direction of the ice sheet surface slope (which also control the ice flow direction). These findings are consistent with the fact that most subglacial lakes are lying close to ice divides and therefore in areas of low surface slopes and high hydraulic fluid potential (Siegert et al., 2007; Pattyn, 2008).

Water circulation along a sloping ice-water interface can produce a glaciohydraulic heat flux that can activate melting and freezing processes at the lake surface (Wuëst and Carmack, 2000) which balance the water influx and outflux of large subglacial lakes in Antarctica (Bell et al., 2002; Tikku et al., 2005). The relatively small size of the Pingualuit subglacial basin should have limited the development of necessary gradients to drive sufficient circulation within the reservoir. The subglacial crater is thus unlikely to be analogous, for example, to the much larger (and not brimful) Lake Vostok (Studinger et al., 2004). At its brimful level, the lake would have most likely behaved as an open water system with water inflows and outflows from the surrounding glacier bed. If not brimful, the subglacial lake would have shrunk to a very small size by net freezing or would have collected meltwater by geothermal melting, as the lake floor lies at a lower elevation than the surrounding glacier bed. When the lake level reached the level of a spillway and if the basal ice was not frozen at the vicinity of the conduit, an outburst flood would occur to release any excess water (e.g. Clarke et al., 2005).

By revealing that the Pingualuit Crater is a suitable subglacial basin for the storage of subglacial water, the modeling findings also suggest that the sediments deposited in the lake may have been preserved from glacial erosion during glacial periods.

5.2. Ice sheet impact on sedimentation (Facies IV and III)

Facies IV and III present a range of ^{14}C ages between 35 740 ± 710 and 28 510 ± 510 cal BP (Fig. 4, Table 1). Within these facies, $\delta^{13}C$ values display more pronounced variability and higher values than in organic-rich intervals. This is the result of external inputs of organic particles from the catchment area or from the littoral zone of the lake (Meyers, 1997; Meyers and Teranes, 2001). Because the

lake has no tributary and no soils has been developed on the internal slopes of the crater (e.g. Fig. 2), glacial motion is the most likely transport agent for these organic particles. Furthermore, the external input of U-rich material in the Payne dispersal train (Daigneault, 2008) is also indicative of distally and glacially derived material in the Crater Lake basin. Several age reversals observed in both facies, as well as the age range obtained (Fig. 4, Table 1) strongly suggest that AMS ^{14}C dating does not adequately represent the depositional time of these organic-poor glacigenic sediments. The latter were more likely deposited just before the final deglaciation of the lake (see section 5.4). The ^{14}C ages in facies III and IV therefore represent a "mixing age" between a recent (e.g. Holocene) and much older (early to mid-Wisconsinan) organic contribution. This reworking process is also apparent from the IRSL results of sample IRSL-B (762–764 cm, Fig. 4), as the AF-corrected natural luminescence suggests dose saturation, typical of feldspar grains that would have never been exposed to sunlight. The saturation of IRSL is thus coherent with sediment being reworked from till or waterlaid sediment that was buried without proper bleaching.

Glacial till found outside the crater is known to be exceptionally rich in pollen because sediments situated at the center of northern Ungava were protected from intense glacial erosion throughout successive glaciations (Richard et al., 1991; Fréchette et al., 1996). According to these authors, these basal till remaining after each glaciation would passively incorporate and preserve pollen grains during warm periods. The material reworked during glaciations would also include terrestrial organic particles (e.g. mosses) from warm periods (Fréchette et al., 1996). Pollen analysis in facies IV and III revealed a relatively high abundance of *Picea* and *Pinus* sp. grains (Girard-Cloutier, 2010). The pollen of these two species are found in the nearby tills (Richard et al., 1991) and therefore reflect their remobilization and incorporation from former interglacial/interstadial periods at the base of the ice sheet and their deposition in the lake during later deglaciation. However, it is unlikely that the same till in the crater surroundings acted as traps and preserved lacustrine diatoms from older interglacials in a similar manner, as neither diatoms nor any other lacustrine sediment vestiges were reported in the regional till (Grönlund et al., 1990; Fréchette et al., 1996). Therefore, the diatoms preserved in the Pingualuit Crater sedimentary sequence more likely reflect the environmental conditions (e.g. ice cover) that occurred during their deposition, even if they are mixed with glacially derived material.

5.3. Deglacial history (Facies IV and III)

The very high density values measured in facies IV, the high abundance of dropstones and the lowest organic carbon and BSi contents in the core in conjunction with the dominance of *Aulacoseira* spp. (Black et al., 2010), a diatom genus known to be able to grow under a thin ice cover (Bondarenko et al., 2006), mark the end of subglacial conditions at the coring site and the onset of proglacial conditions in a proximal environment (Fig. 7C).

Facies IIIb (780–710 cm) is defined by the deposition of some finer-grained, folded and faintly laminated sediments suggesting a turbulent glacigenic sediment flow related to the melting of the ice sheet. Nevertheless, the slightly higher values of BSi and TOC associated with slightly lower $\delta^{13}C$ values (Fig. 5) in this interval indicate an increase of algal productivity (mainly diatoms) likely related to a temporary disappearance of the ice cover at least during part of the year. The dominance of the pollen Cyperaceae (Girard-Cloutier, 2010) and the abundance of several open water planktonic diatom
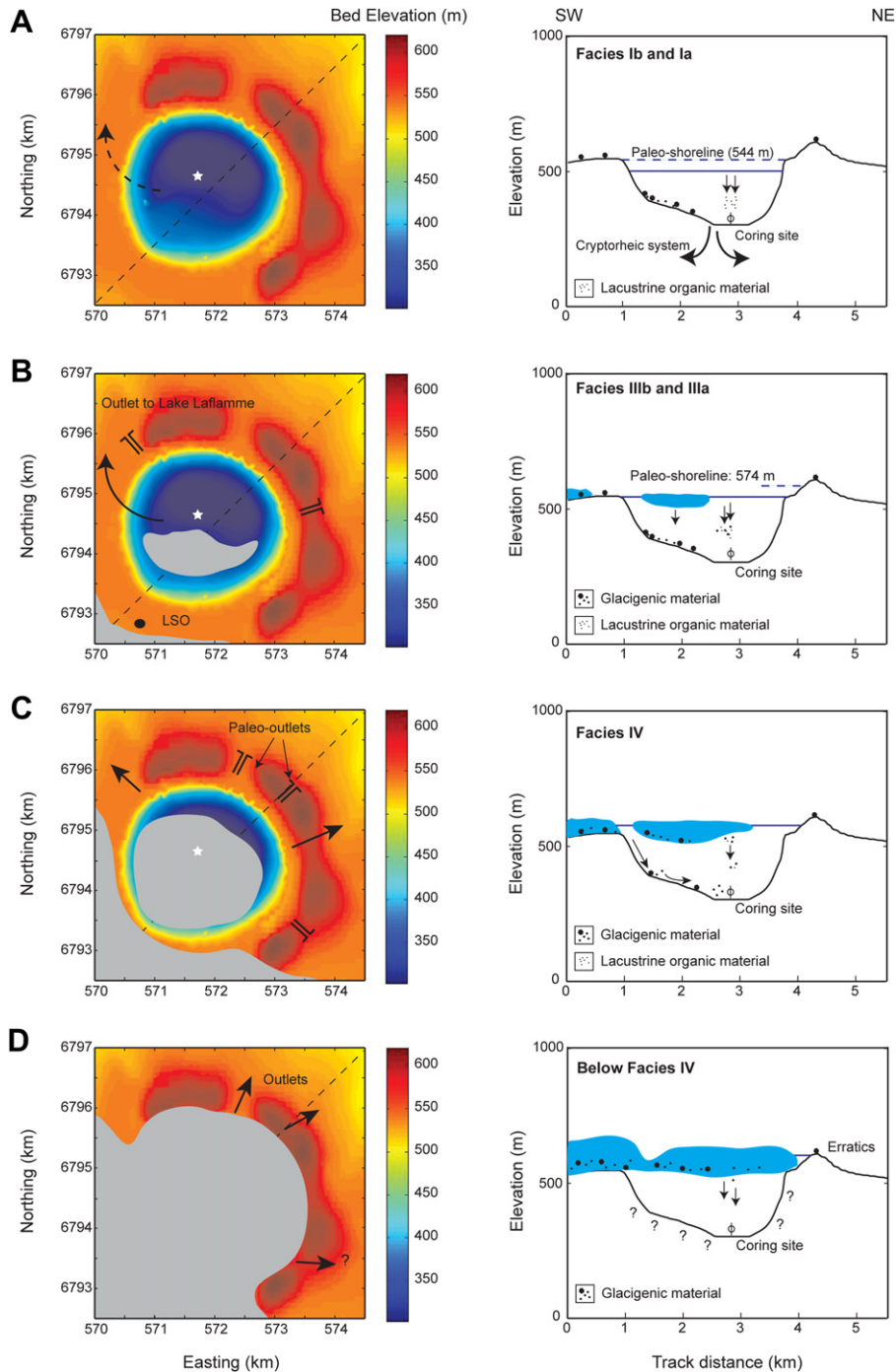
Fig. 7. Conceptual model for sedimentation in Pingualuit Crater Lake since the last deglaciation. Also illustrated are the paleo-lake level drops related to rapid water discharges through different valleys (see section 2.4) according to Bouchard and Saarnisto (1989). Right panels show the situation along SW–NE profile (dashed line on left panels). LSO: Lake du Sud-Ouest on panel B.

species (e.g. *Cyclotella* sp.), as well as the decrease of *Aulacoseira* spp. (Black et al., 2010, in press) also points to temporarily ice-free conditions preceding the final deglaciation of the area. Furthermore, Fe is mobilized during redox-related diagenesis and elevated Fe is commonly observed in oxic or formerly oxic parts of the sediments (Croudace et al., 2006). Higher values of Fe/Ti in facies IIIb may thus indicate the development of a redox front at the sediment/water interface associated with a better oxygenation of the bottom water. This is related to the mixing of the whole water column, which can only occur during ice-free periods in cold monomictic lakes (Lewis Jr., 1983). The depositional transition observed around 780 cm likely marks a major change in predominant depositional mechanisms from a proximal proglacial environment with permanent thin ice cover to a more distal proglacial environment with temporarily ice-free conditions (Fig. 7B). The microfossils and ^{14}C dates obtained in facies IIIb (~34 ka cal BP, Table 1) could reflect a short period of regional ice-free conditions during the mid-Wisconsinan late marine isotopic stage 3 (MIS 3), since Kirby and Andrews (1999) and Andrews and MacLean (2003) suggested that Hudson Strait may have been at least partially deglaciated <34 ka. Recent studies also indicate ice-free conditions during MIS 3 in Fennoscandia (e.g. Helmens and Engels, 2010; Wohlfarth, 2010). However, since the ^{14}C ages correspond to apparent ages and the IRSL age in this interval reflects sediment buried without proper bleaching (see section 5.2), and because of the geographical position of the crater, this interpretation is very speculative at this stage.

The overlying finely laminated silty (rhythmites; <1–2 mm) melt-out deposits (Facies IIIa) are intercalated by massive sand layers (Figs. 4 and 5) and are again characterized by radiocarbon ages between 28 510 ± 510 and 35 740 ± 710 cal BP showing reversals (Fig. 4 and Table 1). This interval is also marked by the decrease of *Cyclotella* sp. and the increase of *Aulacoseira* spp. (Black et al., 2010), both indicative of the presence of a semi-permanent ice cover on the lake. Low TOC and BSi values indicate a very weak primary productivity. The presence of massive sand layers and dropstones, the inclination of the laminae, as well as the high density of these glacigenic sediments all point to high meltwater and sediment discharges. The top of this unit includes more horizontal rhythmites reflecting a lower energetic depositional environment, associated with the decay of the remnant glacier and with weaker influence of the ice sheet-derived detritic inputs (Fig. 7B). Moreover, the increasing trend of Fe/Ti indicates a slight evolution of redox-related diagenetic conditions at the sediment/water interface, likely associated with a better oxygenation of the bottom water and a higher mixing of the water column related to shorter ice cover periods. Facies IV and IIIa thus reflect original glacigenic sediments deposited in a subglacial and lacustrine environment by ice shedding from the disintegrating glacier above during the last stages of deglaciation (Fig. 7C and B).

5.4. Postglacial history (Facies I)

Without any major terrestrial vegetation in the catchment area of this Canadian Arctic Crater Lake, the increase of TOC associated with the lower values of δ^{13}C of the organic matter in facies I reflects an increase of the lacustrine (mainly algal) productivity. Similarly, the higher BSi concentrations reflect the lacustrine productivity bloom of siliceous algae (Black et al., 2010) related to ice-free conditions (Figs. 5 and 7A). Pollen analyses reveal the development of a shrub tundra (Girard-Cloutier, 2010) also indicative of a warmer climate. Furthermore, high values of Fe/Ti, associated with the development of a redox front, suggest ventilation and strongly support the absence of a permanent ice cover.

The onset of organic sedimentation at 270 cm blf (Facies Ib) marks the cessation of glacial inputs as the result of the

disappearance of last remnants of the LIS and occurred ca. 6000 ± 40 yr BP (6844 ± 100 cal BP) (Figs. 4 and 8). The top of the interval is estimated at 5000 ± 40 yr BP (5760 ± 135 cal BP), assuming a constant sedimentation rate between treated ages (Fig. 8 and Table 1) of 12 cm/ka. The thin compact inorganic clayish layer observed below the facies Ib likely corresponds to the deposition by settling of fine particles after the final melting of the vestigial lake ice pan, as also suggested by the IRSL apparent ages obtained for sample IRSL-A (Fig. 4). The IRSL properties of the aliquots used for measurements indicate bleaching by sunlight prior to final deposition, and the coarse grained feldspars yielded a combined age of 74 ka (±9 ka) whereas the fine grains suggest a somewhat similar age of 66 ka (±10 ka). This IRSL age estimation likely indicates that some grains were incorporated at the base of the ice sheet since the beginning of the last glaciation (Clark et al., 1993) and were never exposed to sunlight since that time. The IRSL apparent age thus once again reflects a mixed age, resulting from the incorporation of feldspar grains of various ages from the regional extra-crater surface. Due to the large size of the retention basin and the low regional glacial movements, these grains were directly introduced into the lake basin during deglaciation. The IRSL age of these grains thus reflects the time when they were buried prior to the last glaciation and not the age of their deposition in the lake, whereas the age of the algal organic matter produced in the lake at that time rather reflects the onset of deglaciation. This further indicates that the area has not been deglaciated since the onset of the last glaciation. The onset of ice-free conditions allowed a productivity surge and the organic matter produced in the lake was adsorbed onto the mineral particles dated by IRSL during their decantation.

The change from proglacial to postglacial conditions in the Pingualuit Crater Lake basin indicates the final collapse of the LIS at 6850 cal BP and confirms that it was one of the last sites to become ice-free in this part of the eastern Canadian Arctic. This scenario is consistent with the main thrust of data available for eastern Canada that reveal cold temperatures during the early postglacial, followed by warming at 6850 cal BP (e.g. Andrews, 1972, 1973; Richard et al.,
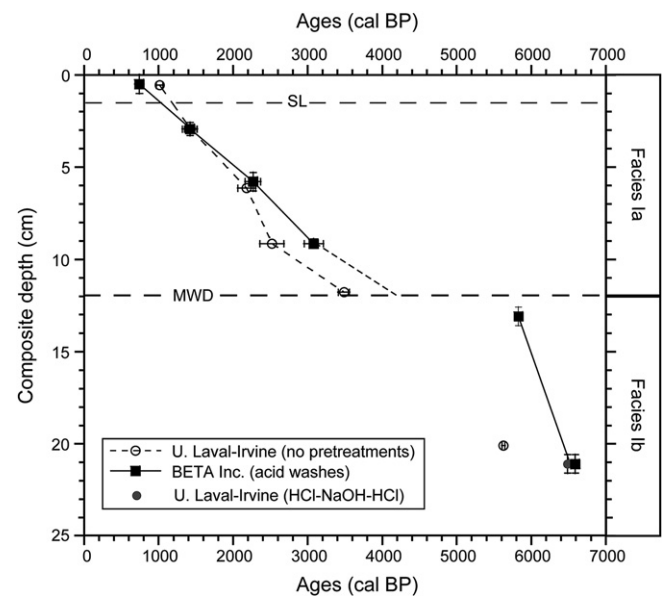

Fig. 8. Age-depth relationship for the last 6850 cal BP. The composite depth was constructed by excluding mass wasting events and glacigenic sediments from the profile (see text for details). SL: sandy layer in the surface core; MWD: erosive mass wasting deposit (facies II).

1982; Williams et al., 1995; Levac and de Vernal, 1997; Andrews et al., 1995; Sawada et al., 1999; Kerwin et al., 1999, 2004; Kaplan et al., 2002; Saulnier-Talbot and Pienitz, 2009). This major regional change could thus be linked to the final disappearance of the LIS.

5.5. Mass wasting deposit (Facies II) and age-depth model since the deglaciation

The sharp contact observed at 257 cm on CAT-Scan images and recorded by both drastic geochemical and physical variations marks the base of a Mass Wasting Deposit (MWD; facies II), characterized on the seismic profile by a transparent acoustic facies (Fig. 3B). Some apparent radiocarbon ages measured in the sediments of facies II are also similar to the radiocarbon ages obtained in facies IV and III, which correspond to deglacial/proglacial sediments (see section 5.3). Furthermore, the sharp decrease of Fe/Ti reflects the rapid deposition of the MWD that prevented a redox front to migrate upward at the base of the MWD. The thin compact clay layer present at the base of the deposit may indicate some fluidization related to the occurrence of this sedimentary event. The MWD is mainly composed of folded and reworked glacigenic material, as indicated by some ^{14}C AMS dating and also by the similarity of its physical properties with facies IIIa (gamma density, magnetic susceptibility, Fe/Ti, TOC and δ^{13}C values; Fig. 5, Table 1). This MWD has affected the entire deep basin as shown on the seismic profile (Fig. 3B) by the extent of the transparent acoustic facies. CAT-Scan and X-ray images indicate that part of the internal sedimentary organization (fine laminations) has been preserved, suggesting a translational slide (Mulder and Cochonnat, 1996).

Based on the sedimentary physical and geochemical properties, the X-ray and CAT-Scan images and ^{14}C ages, we place the upper boundary of the MWD at 13.5 cm in the surface core, associated with an age of 4200 cal BP (Fig. 8). A radiocarbon age obtained immediately below the lower contact of the MWD in the piston core confirms that this event was erosive and that a hiatus is observed between 4200 and 5750 cal BP (Fig. 8). The thin inorganic, compact clayish layer immediately below the upper boundary of the MWD (14.5–13.5 cm) reflects the settling of the fine particles following the sedimentary event, while the dense sediments between 17 and 14.5 cm likely correspond to a former sediment/water interface, as indicated by the high Fe/Ti ratio. This further supports the hypothesis of a translational slide. The younger ages obtained on the last 3 cm at the disturbed base of the surface core (Table 1), already observed in other Ungava lake archives (e.g. Saulnier-Talbot and Pienitz, 2009) could reflect a coring artifact due to core handling and capping.

The slide occurred around 4200 cal BP, when the surface connection with Lake Laflamme (Bouchard and Saarnisto, 1989) was possibly still active (Fig. 7A). As the LIS decayed, its geometry evolved and the ice margin would have receded toward the site of the subglacial lake. As the distance to the ice margin decreased, the ice-surface slope above the lake would have increased causing the lake volume to shrink. At the same time, the reduced ice thickness would reduce water pressure in the lake, whereas the pressure of pore fluids in low permeability sediments would remain high and could promote slope instability. The MWD could thus be related to slope instabilities associated with the rapid exorheic drainage through channels observed on the outer crater rim following the deglaciation (see section 2.4).

Another trigger mechanism of the MWD could have been an earthquake, as the area is seismically active and was struck by a $M_S = 6.3$ earthquake in 1989 (Adams et al., 1991). The latter occurred close to the surface around 120 km southwest of the crater (60.12°N; 73.60°W) and was the first reported intraplate earthquake in eastern North America known to have produced surface faulting (10 km long surface rupture; Adams et al., 1991). Moreover, as in Scandinavia (Mörner, 2005), increased seismic activity associated with glacio-isostatic rebound following the deglaciation could have occurred in Ungava. Postglacial land emergence in the Salluit region was characterized by a phase of rapid initial glacio-isostatic rebound averaging about 8 m 100 a^{-1} until 5200 yr BP, followed by a period of much slower uplift with average rates <0.3 m 100 a^{-1} (Matthews, 1966, 1967; Gray et al., 1993). Unfortunately, no data are available for glacio-isostatic rebound in the Kangiqsujuaq region, but the crater area has an uplift rate of about 0.4 m 100 a^{-1} since 1 ka BP (Matthews, 1967).

By excluding this MWD and the small sand layer at the top of the surface core, we calculate that about 25 cm of sediments have been deposited since the final collapse of the LIS ca. 6850 cal BP (Fig. 8). The composite age-depth model indicates a higher mean sedimentation rate following deglaciation (∼12 cm/ka) than during the late Holocene (<3 cm/ka). This is probably directly linked to the decreased influence of glacially derived meltwaters. The mean sedimentation rate inferred for the late Holocene is comparable with previous estimates based on one ^{14}C date (5780 ± 135 cal BP) at 14 cm depth (Bouchard et al., 1989a), indicating a mean sedimentation rate of ca. 2.4 cm/ka. These very low sedimentation rates reflect the small and rocky catchment area and explain the exceptional clarity of the lake water, its high light penetration, as well as its extremely low nutrient contents.

6. Conclusions

We present evidence that Pingualuit Crater Lake existed as a subglacial lake beneath the Laurentide Ice Sheet at least during the last glaciation and that its bottom sediments escaped glacial erosion and may archive a unique long-term continental paleorecord of the Canadian Arctic. Sediments retrieved mostly contain a mixture of information extracted from the past interglacial and glacial periods and reworked by glacial activity. The inorganic dense grey and sandier sediments are interpreted as glacigenic material related to the last deglaciation and reflect original depositional conditions in a subglacial and lacustrine environment. Organic-rich intervals correspond to ice-free conditions associated with the postglacial period. If other study sites in such low productivity environments suffer from old carbon effects, this new sedimentary record from northernmost Ungava has produced a reliable new means of dating the disappearance of the last remnants of the Laurentide Ice Sheet at 6850 cal BP, which coincides with a major climatic and environmental transition throughout the eastern Canadian Arctic. Nevertheless, the paleoclimatic reconstructions from the Pingualuit Crater Lake sedimentary sequence are complicated by the importance of mass wasting events and glacigenic sediments as well as by the low sedimentation rates during ice-free periods.

References

Abbott, M.B., Stafford Jr., T.W., 1996. Radiocarbon geochemistry of modern and ancient Arctic lake systems, Baffin Island, Canada. Quaternary Research 45, 300–311.

Arctic Climate Impact Assessment (ACIA), 2004. Impacts of a Warming Arctic. Arctic Climate Impact Assessment. Cambridge University Press, 144 pp.

Adams, J., Wetmiller, R.J., Hasegawa, H.S., Drysdale, J., 1991. The first surface faulting from a historical intraplate earthquake in North America. Nature 352, 617–618.

Andrews, J.T., 1972. Recent and fossil growth rates of marine bivalves, Canadian Arctic, and Late-Quaternary Arctic marine environments. Palaeogeography, Palaeoclimatology, Palaeoecology 11, 157–176.

Andrews, J.T., 1973. Late Quaternary variation in oxygen and carbon isotopic compositions in Canadian Arctic marine bivalves. Palaeogeography, Palaeoclimatology, Palaeoecology 14, 187–192.

Andrews, J.T., MacLean, B., 2003. Hudson Strait ice streams: a review of stratigraphy, chronology and links with North Atlantic Heinrich events. Boreas 32, 4–17.

Andrews, J.T., MacLean, B., Kerwin, M., Manley, W., Jennings, A.E., Hall, F., 1995. Final stages of the collapse of the Laurentide Ice Sheet, Hudson Strait, Canada, NWT: ^{14}C AMS dates, seismic stratigraphy, and magnetic susceptibility logs. Quaternary Science Reviews 14, 983–1004.

Auclair, M., Lamothe, M., Huot, S., 2003. The measurement of anomalous fading for feldspar IRSL using SAR. Radiation Measurements 37, 487–492.

Axford, Y., Briner, J.P., Cooke, C.A., Francis, D.R., Michelutti, N., Miller, G.H., Smol, J.P., Thomas, E.K., Wilson, C.R., Wolfe, A.P., 2009. Recent changes in a remote Arctic lake are unique within the past 200,000 years. Proceedings of the National Academy of Sciences 106, 18443–18446.

Bell, R.E., Studinger, M., Tikku, A.A., Clarke, G.K.C., Gutner, M.M., Meertens, C., 2002. Origin and fate of Lake Vostok water frozen to the base of the East Antarctic ice sheet. Nature 416, 307–310.

Black, J.L., Hausmann, S., Pienitz, R., St-Onge, G., Guyard, H., Salonen, V.-P., Lavoie, M., Girard-Cloutier, A.-M., Luoto, T., 2010. Reconstruction of Paleoenvironmental Changes from Pingualuit Crater Lake Sediments during Glacial-interglacial Cycles MIS 1 to MIS 8: A Long-term Terrestrial Record from the Canadian Arctic. European Geophysical Union, Vienna, Austria.

Black, J.L., Edlund, M.B., Hausmann, S., Pienitz, R. Small freshwater thalassiosiroid diatoms from Pingualuit Crater Lake, northern Québec and description of Cyclotella pingualuitii sp. nov. Diatom Research, in press.

Bondarenko, N.A., Timoshkin, O.A., Röpstorf, P., Melnik, N.G., 2006. The under-ice and bottom periods in the life cycle of Aulacoseira baicalensis (K. Meyer) Simonsen, a principal Lake Baikal alga. Hydrobiologia 568, 107–109.

Bouchard, M.A., 1989a. Stratigraphie et sédimentation sous- et pro-glaciaire au lac du cratère du Nouveau-Québec. In: Bouchard, M.A. (Ed.), L'histoire naturelle du Cratère du Nouveau-Québec. Collection Environnement et Géologie, vol. 7. Université de Montréal, pp. 225–235.

Bouchard, M.A., 1989b. Englaciation et glaciation du cratère du Nouveau-Québec, un modèle théorique. In: Bouchard, M.A. (Ed.), L'histoire naturelle du Cratère du Nouveau-Québec. Collection Environnement et Géologie, vol. 7. Université de Montréal, pp. 139–163.

Bouchard, M.A., Marcotte, C., 1986. Regional Glacial Dispersal Patterns in Ungava, Nouveau-Québec. Geological Survey of Canada. paper 86–1B, 295–304.

Bouchard, M.A., Marsan, B., 1989. Description générale du cratère du Nouveau-Québec. In: Bouchard, M.A. (Ed.), L'histoire naturelle du Cratère du Nouveau-Québec. Collection Environnement et Géologie, vol. 7. Université de Montréal, pp. 37–58.

Bouchard, M.A., Saarnisto, M., 1989. Déglaciation et paléo-drainages du cratère du Nouveau du Québec. In: Bouchard, M.A. (Ed.), L'histoire naturelle du Cratère du Nouveau-Québec. Collection Environnement et Géologie, vol. 7. Université de Montréal, pp. 165–189.

Bouchard, M.A., Péloquin, S., Fortin, G., 1989a. L'échantillonnage des sédiments au fond du lac du cratère − 1986. In: Bouchard, M.A. (Ed.), L'histoire naturelle du Cratère du Nouveau-Québec. Collection Environnement et Géologie, vol. 7. Université de Montréal, pp. 191–198.

Bouchard, M.A., Marsan, B., Péloquin, S., Fortin, G., Saarnisto, M., Shilts, W.W., David, P.P., Fliszár, A., 1989b. Géologie glaciaire du cratère du Nouveau-Québec. In: Bouchard, M.A. (Ed.), L'histoire naturelle du Cratère du Nouveau-Québec. Collection Environnement et Géologie, vol. 7. Université de Montréal, pp. 101–138.

Bruneau, D., Gray, J.T., 1997. Ecoulements glaciaires et déglaciation hâtive (ca 11 ka BP) du nord-est de la péninsule d'Ungava, Québec, Canada. Canadian Journal of Earth Sciences 34, 1089–1100.

CAPE Last Interglacial Project Members, 2006. Last Interglacial Arctic warmth confirms polar amplification of climate change. Quaternary Science Reviews 25, 1383–1400.

Clark, P.U., Clague, J.J., Curry, B.B., Dreimanis, A., Hicock, S.R., Miller, G.H., Berger, G.W., Eyles, N., Lamothe, M., Miller, B.B., Mott, R.J., Oldale, R.N., Stea, R.R., Szabo, J.P., Thorleifson, L.H., Vincent, J.S., 1993. Initiation and development of the Laurentide and Cordilleran ice sheets following the last interglaciation. Quaternary Science Reviews 12, 79–114.

Clarke, G.K.C., 2005. Subglacial processes. Annual Reviews of Earth and Planetary Sciences 33, 247–276.

Clarke, G.K.C., Leverington, D.W., Teller, J.T., Dyke, A.S., Marshall, S.J., 2005. Fresh arguments against the Shaw megaflood hypothesis. Quaternary Science Reviews 24, 1533–1541.

COHMAP members, 1988. Climatic changes of the last 18 000 years: observations and model simulations. Science 241, 1043–1052.

Cohen, A.S., 2003. Paleolimnology: The History and Evolution of Lake Systems. Oxford University Press, New York, 500 pp.

Comiso, J.C., 2003. Warming trends in the Arctic from Clear-Sky Satellite observations. Journal of Climatology 16, 3498–3510.

Croudace, I.W., Rindby, A., Rothwell, R.G., 2006. ITRAX: description and evaluation of a new multi-function X-ray core scanner. In: Rothwell, R.G. (Ed.), New Techniques in Sediment Core Analysis. Geological Society, London, pp. 51–63.

Currie, K.L., 1965. The geology of the New Quebec crater. Canadian Journal of Earth Sciences 2, 141–160.

Currie, K.L., Dence, M.R., 1963. Rock deformation in the rim of the New Quebec crater, Canada. Nature 198, 80.

Daigneault, R.-A., 1997a. Géologie du Quaternaire du Nord du Nunavik, Québec. PhD thesis, Montréal, Université de Montréal, 210 pp.

Daigneault, R.-A., 1997b. Géologie des formations en surface, région du cap de Nouvelle-France, du cratère du Nouveau-Québec et de Kangiqsujuaq, Québec-Territoires du Nord-Ouest. Commission géologique du Canada. Carte 1863A, échelle 1/250 000.

Daigneault, R.-A., 2008. Géologie du Quaternaire du nord de la péninsule d'Ungava, Québec. Commission géologique du Canada, bulletin 533, 115.

Daigneault, R.-A., Bouchard, M.A., 2004. Les écoulements et le transport glaciaires dans la partie septentrionale du Nunavik (Québec). Canadian Journal of Earth Sciences 41, 919–938.

Delisle, C.E., Roy, L., 1989. L'Omble chevalier (Salvelinus alpinus) du lac du cratère du nouveau Québec. In: Bouchard, M.A. (Ed.), L'histoire naturelle du Cratère du Nouveau-Québec. Collection Environnement et Géologie, vol. 7. Université de Montréal, pp. 261–276.

Dyke, A.S., 2004. An outline of North American deglaciation with emphasis on central and northern Canada. In: Ehlers, J., Gibbard, P.L. (Eds.), Quaternary Glaciation - Extent and Chronology, Part II. Developments in Quaternary Science, vol. 26. Elsevier, Netherlands, pp. 373–424.

Dyke, A.S., Prest, V.K., 1987. Late Wisconsinan and Holocene history of the Laurentide ice sheet. Géographie Physique et Quaternaire 41, 237–263.

Dyke, A.S., Andrews, J.T., Clark, P.U., England, J.H., Miller, G.H., Shaw, J., Veillette, J.J., 2002. The Laurentide and Innuitian ice sheets during the last glacial maximum. Quaternary Science Reviews 21, 9–31.

Francus, P., Lamb, H., Nakagawa, T., Marshall, M., Brown, E., Suigetsu 2006 Project Members, 2009. The potential of high-resolution X-ray fluorescence core scanning: applications in paleolimnology. PAGES News 17 (3), 93–95.

Fréchette, B., Bouchard, M.A., Richard, P.J.H., 1996. Le till pollinifère de la péninsule du Nunavik, Québec septentrional. Géographie physique et Quaternaire 50 (3), 331–340.

Gantner, N., Veillette, J., Michaud, W.K., Bajno, R., Muir, D., Vincent, W.F., Power, M., Dixon, B., Reist, J.D., Pienitz, R., Hausmann, S. Physical and biological factors affecting mercury and perfluorinated contaminants in Arctic char (Salvelinus alpinus) of Pingualuk Crater Lake (Nunavik, Canada). Arctic, submitted for publication.

Girard-Cloutier, A-M., 2010. Reconstitution paléobotanique et paléoclimatique en Ungava: analyse pollinique des sédiments du Cratère des Pingualuit. M.Sc thesis, Université Laval, Département de géographie, 68 pp.

Gray, J.T., 2001. Patterns of ice flow and deglaciation chronology for southern coastal margins of Hudson Strait and Ungava Bay. In: MacLean, B.S. (Ed.), Marine Geology of Hudson Strait and Ungava Bay, Eastern Arctic Canada: Late Quaternary Sediments, Depositional Environments, and Late Glacial–deglacial History Derived from Marine and Terrestrial Studies. Geological Survey of Canada Bulletin, pp. 31–55.

Gray, J.T., Lauriol, B., 1985. Dynamics of the late Wisconsin ice sheet in the Ungava Peninsula interpreted from geomorphological evidence. Arctic and Alpine Research 17, 289–310.

Gray, J.T., Lauriol, B., Bruneau, D., Ricard, J., 1993. Postglacial emergence of Ungava Peninsula, and its relationship to glacial history. Canadian Journal of Earth Sciences 30, 1676–1696.

Grieve, R.A.F., Bottomley, R.B., Bouchard, M.A., Robertson, P.B., Orth, C.J., Attrep, M., 1991. Impact melt rocks from New Quebec crater, Quebec, Canada. Meteoritics 26, 31–39.

Grönlund, T., Lortie, G., Guilbault, J.-P., Bouchard, M.A., Saarnisto, M., 1990. Diatoms and arcellaceans from Lac du Cratère du Nouveau-Québec, Ungava, Québec, Canada. Canadian Journal of Botany 68, 1187–1200.

Guyard, H., Chapron, E., St-Onge, G., Anselmetti, F.S., Arnaud, F., Magand, O., Francus, P., Mélières, M.-A., 2007. High-altitude varve records of abrupt environmental changes and mining activity over the last 4000 years in the Western French Alps (Lake Bramant, Grandes Rousses Massif). Quaternary Science Reviews 26, 2644–2660.

Helmens, K.F., Engels, S., 2010. Ice-free conditions in eastern Fennoscandia during early Marine Isotope Stage 3: lacustrine records. Boreas 39, 399–409.

Janssen, K.N., 2003. Early Holocene glacial lakes and ice marginal retreat pattern in Labrador/Ungava, Canada. Palaeogeography, Palaeoclimatology, Palaeoecology 193, 473–501.

Kaplan, M.R., Wolfe, A.P., 2006. Spatial and temporal variability of Holocene temperature in the North Atlantic region. Quaternary Research 65, 223–231.

Kaplan, M.R., Wolfe, A.P., Miller, G.H., 2002. Holocene environmental variability in Southern Greenland inferred from lake sediments. Quaternary Research 58, 149–159.

Kaufman, D.S., Ager, T.A., Anderson, N.J., Anderson, P.M., Andrews, J.T., Bartlein, P.J., Brubaker, L.B., Coats, L.L., Cwynar, L.C., Duvall, M.L., Dyke, A.S., Edwards, M.E., Eisner, W.R., Gajewski, K., Geirsdottir, A., Hu, S., Jennings, A.E., Kaplan, M.R., Kerwin, M.W., Lozhkin, A.V., MacDonald, G.M., Miller, G.H., Mock, C.J., Oswald, W.W., Otto-Bliesner, B.L., Porinchu, D.F., Ruhland, K., Smol, J.P., Steig, E.J., Wolfe, B.B., 2004. Holocene thermal maximum in the western Arctic (0–180°W). Quaternary Science Reviews 23, 529–560.

Kerwin, M.W., Overpeck, J.T., Webb, R.S., de Vernal, A., Rind, D.H., Healy, R.J., 1999. The role of oceanic forcing in mid-Holocene Northern Hemisphere climatic change. Paleoceanography 14 (2), 200–210.

Kerwin, M.W., Overpeck, J., Webb, R., Anderson, K.H., 2004. Pollen-based summer temperature reconstructions for the eastern Canadian Boreal Forest, sub-Arctic and Arctic. Quaternary Science Reviews 23, 1901–1924.

Kirby, M.E., Andrews, J.T., 1999. Mid-Wisconsin Laurentide ice sheet growth and decay: implications for Heinrich events-3 and -4. Paleoceanography 14, 211–223.

Lamothe, M., 2004. Optical dating of pottery, burnt stones, and sediments from selected Quebec archaeological sites. Canadian Journal of Earth Sciences 41, 659–667.

Lamothe, M., Auclair, M., Hamzaoui, C., Huot, S., 2003. Towards a prediction of long-term anomalous fading of feldspar IRSL. Radiation Measurements 37, 493–498.

Lauriol, B., Gray, J.T., 1987. The decay and disappearance of the late Wisconsin ice sheet in the Ungava Peninsula, northern Québec, Canada. Arctic and Alpine Research 19, 109–126.

Ledoux G., Lajeunesse P., Philibert G., Sinkunas B., Guyard H., St-Onge G., Hausmann S., Pienitz R., 2011. Morpho-stratigraphy of Pingualuit Crater Lake, Ungava Peninsula, Nunavik. 41th Arctic Workshop, Montréal, Canada, p. 179.

Levac, E., de Vernal, A., 1997. Postglacial changes of terrestrial and marine environments along the Labrador coast: palynological evidence from cores 91-045-005 and 91-045-006, Cartwright Saddle. Canadian Journal of Earth Sciences 34 (10), 1358–1365.

Lewis Jr., W.M., 1983. A revised classification of lakes based on mixing. Canadian Journal of Fisheries and Aquatic Sciences 40, 1779–1787.

Marshall, S.J., Tarasov, L., Clarke, G.K.C., Peltier, W.R., 2000. Glaciological reconstruction of the Laurentide Ice Sheet: physical processes and modeling challenges. Canadian Journal of Earth Sciences 37, 769–793.

Marshall, S.J., James, J.T.S., Clarke, G.K.C., 2002. North American ice sheet reconstructions at the last glacial maximum. Quaternary Science Reviews 21, 175–192.

Martin, N.V., 1955. Limnological and biological observations in the region of the Ungava or Chubb crater, province of Québec. Journal of the Fisheries Research Board of Canada 12, 487–496.

Matthews, B., 1963. Glacial geomorphological investigations in northern Ungava, Québec, Canada. Ice 12, 9–10.

Matthews, B., 1966. Radiocarbon dated postglacial land uplift in Northern Ungava, Canada. Nature 211, 1164–1166.

Matthews, B., 1967. Late Quaternary land emergence in northern Ungava, Québec. Arctic 20, 176–202.

Ministère du Développement Durable, de l'Environnement et des Parcs (MDDEP), 2005. Plan directeur, Parc national des Pingualuit, ISBN 2-550-45007-8 Envirodoq ENV/2005/0173.

Meyers, P.A., 1997. Organic geochemical proxies of paleoceanographic, paleolimnologic and paleoclimatic processes. Organic Geochemistry 27 (5–6), 213–250.

Meyers, P.A., Teranes, J.L., 2001. Sediment organic matter. Physical and geochemical methods. In: Last, W.M., Smol, J.P. (Eds.), Tracking Environmental Change Using Lake Sediments, vol. 2. Kluwer Academic Publishers, Dordrecht, pp. 239–269.

Mörner, N.-A., 2005. An interpretation and catalogue of paleoseismicity in Sweden. Tectonophysics 408, 265–307.

Moussawi, A., Tessier, G., 1989. L'épaisseur des sédiments au fond du Lac du Cratère du Nouveau-Québec: relevés géophysiques. In: Bouchard, M.A. (Ed.), L'Histoire Naturelle du Cratère du Nouveau-Québec. Collection Environnement et Géologie, vol. 7. Université de Montréal, pp. 199–222.

Mulder, T., Cochonnat, P., 1996. Classification of offshore mass movements. Journal of Sedimentary Research 66, 43–57.

Müller, P.J., Schneider, R., 1993. An automated leaching method for the determination of opal in sediments and particulate matter. Deep-Sea Research 40, 425–444.

Niessen, F., Gebhardt, A.C., Kopsch, C., Wagner, B., 2007. Seismic investigation of the El'gygytgyn impact Crater Lake (Central Chukotka, NE Siberia): preliminary results. Journal of Paleolimnology 37, 49–63.

Otto-Bliesner, B.L., Marshall, S.J., Overpeck, J.T., Miller, G.H., Hu, A., CAPE Last Interglacial Project members, 2006. Stimulating Arctic climate warmth and Icefield retreat in the last interglaciation. Science 311, 1751–1753.

Ouellet, M., Pagé, P., Bouchard, M.A., 1989. Quelques aspects limnologiques du lac du cratère du Nouveau-Québec, Ungava. In: Bouchard, M.A. (Ed.), L'Histoire Naturelle du Cratère du Nouveau-Québec. Collection Environnement et Géologie, vol. 7. Université de Montréal, pp. 238–259.

Overpeck, J., Hughen, K., Hardy, D., Bradley, R., Case, R., Douglas, M., Finney, B., Gajewski, K., Jacoby, G., Jennings, A., Lamoureux, S.K., Lasca, A., MacDonald, G., Moore, J., Retelle, M., Smith, S., Wolfe, A., Zienlinski, G., 1997. Artic environmental change of the last four centuries. Science 278, 1251–1256.

Overpeck, J.T., Otto-Bliesner, B.L., Miller, G.H., Muhs, D.R., Alley, R.B., Kiehl, J.T., 2006. Paleoclimatic evidence for future ice-sheet instability and rapid sea-level rise. Science 331, 1747–1750.

Pattyn, F., 2008. Investigating the stability of subglacial lakes with a full Stokes ice-sheet model. Journal of Glaciology 54 (185), 353–361.

Peltier, W.R., 2002. Global glacial isostatic adjustment: Palaeogeodetic and space-geodetic tests of the ICE-4G (VM2) model. Journal of Quaternary Science 17, 491–510.

Perren, B., Bradley, R.S., Francus, P., 2003. Rapid lacustrine response to recent high Arctic warming: a diatom record from Sawtooth Lake, Ellesmere Island, Nunavut. Arctic, Antarctic, and Alpine Research 35, 271–278.

Pienitz, R., Douglas, M.S.V., Smol, J.P. (Eds.), 2004. Long-term Environmental Change in Arctic and Antarctic Lakes. Developments in Paleoenvironmental Research (DPER), vol. 8. Springer Publishers, Dordrecht, p. 562.

Pienitz, R., Doran, P., Lamoureux, S., 2008. Origin and geomorphology of lakes in the polar regions. In: Vincent, W.F., Laybourn-Parry, J. (Eds.), Polar Lakes and Rivers—Limnology of Arctic and Antarctic Aquatic Ecosystems. Oxford University Press, Oxford, UK, pp. 25–41.

Richard, P.J.H., 1981. Paléophytogéographie postglaciaire en Ungava par l'analyse pollinique. Collection Paléo-Québec 13, 153.

Richard, P.J.H., Larouche, A.C., Bouchard, M.A., 1982. Âge de la déglaciation finale et histoire postglaciaire de la végétation dans la partie centrale du Nouveau-Québec. Géographie physique et Quaternaire 37, 63–90.

Richard, P.J.H., Larouche, A.C., Morasse, N., 1989. Études floristiques et paléo-phytogéographiques au Cratère du Nouveau-Québec. In: Bouchard, M.A. (Ed.), L'Histoire Naturelle du Cratère du Nouveau-Québec. Collection Environnement et Géologie, vol. 7. Université de Montréal, pp. 315–342.

Richard, P.J.H., Bouchard, M.A., Gangloff, P., 1991. The significance of pollen-rich inorganic lake sediments in the Cratère du Nouveau-Québec area, Ungava, Canada. Boreas 20, 135–149.

Saulnier-Talbot, E., Pienitz, R., 2009. Postglacial chironomid assemblage succession in northernmost Ungava Peninsula, Canada. Journal of Quaternary Sciences 25 (2), 203–213.

Saulnier-Talbot, E., Pienitz, R., Stafford Jr., T.W., 2009. Establishing Holocene sediment core chronologies for northern Ungava lakes, Canada, using humic acids (AMS ¹⁴C) and ²¹⁰Pb. Quaternary Geochronology 4, 278–287.

Sawada, M., Gajewski, K., de Vernal, A., Richard, P., 1999. Comparison of marine and terrestrial Holocene climatic reconstructions from northeastern North America. Holocene 9 (3), 267–277.

Siegert, M.J., Le Brock, A., Payne, A.J., 2007. Hydrological connections between Antarctic subglacial lakes and the flow of water beneath the East Antarctic Ice Sheet. In: Hambrey, M.J., Christoffersen, P., Glasser, N.F., Hubbard, B. (Eds.), Glacial Sedimentary Processes and Products. Blackwell Publishing, Oxford, pp. 1–7.

Soille, P., Gratin, C., 1994. An efficent algorithm for drainage network extraction on DEM'S. Journal of Visual Communication and Image Representation 5 (2), 181–189.

St-Onge, G., Long, B., 2009. CAT-scan analysis of sedimentary sequences: an ultrahigh-resolution paleoclimatic tool. Engineering Geology 103, 127–133.

St-Onge, G., Mulder, T., Francus, P., Long, B., 2007. Continuous physical properties of cored marine sediments. In: Hillaire-Marcel, C., de Vernal, A. (Eds.), Proxies in Late Cenozoic Paleoceanography. Elsevier, Netherlands, pp. 63–98.

Studinger, M., Bell, R.E., Tikku, A.A., 2004. Estimating the depth and shape of subglacial Lake Vostok's water cavity from aerogravity data. Geophysical Research Letters 31, L12401. doi:10.1029/ 2004GL019801.

Stuiver, M., Reimer, P.J., Reimer, R.W., 2010. CALIB 6.0.1 [www Program and Documentation]. 14CHRONO Centre, Queen's University Belfast, Belfast. <http://www.calib.org> (accessed 29.11.10).

Taylor, F.C., 1982. Reconnaissance geology of a part of the Canadian Shield, northern Quebec and Northwest Territories. Geological Survey of Canada Memoir 399, 32.

Tikku, A.A., Bell, R.E., Studinger, M., Clarke, G.K.C., Tabacco, I., Ferraccioli, F., 2005. Influx of meltwater to subglacial Lake Concordia, east Antarctica. Journal of Glaciology 51 (172), 96–104.

Williams, K.M., Short, S.K., Andrews, J.T., Jennings, A.E., Mode, W.N., Syvitski, J.P.J., 1995. The eastern Canadian Arctic at ca. 6 ka BP: a time of transition. Géographie Physique et Quaternaire 49, 13–27.

Wohlfarth, B., 2010. Ice-free conditions in Sweden during marine Isotope stage 3? Boreas 39 (2), 377–398.

Wolfe, A.P., Miller, G.H., Olsen, C.A., Forman, S.L., Doran, P.T., Holmgren, S.U., 2004. Geochronology of high latitude Lake sediments. In: Pienitz, R., Douglas, M.S.V., Smol, J.P. (Eds.), Long-term Environmental Change in Arctic and Antarctic Lakes. Springer, Dordrecht, pp. 19–52.

Wüest, A., Carmack, E., 2000. A priori estimates of mixing and circulation in the hard-to-reach water body of Lake Vostok. Ocean Modelling 2, 29–43.